International Journal of Networks and Communications 2018, 8(3): 43-62
DOI: 10.5923/j.ijnc.20180803.01

Transmission Performance of Unamplified 1310 nm PAM-Based Data Center Optical Interconnects

Duha S. Ahmed*, Raad S. Fyath

Department of Computer Engineering, Al-Nahrain University, Baghdad, Iraq

Abstract Optical links incorporating multilevel pulse amplitude modulation (PAM) with intensity modulation/direct detection (IM/DD) scheme have shown promising features when used as low-cost data center interconnects. This paper addresses the transmission performance of PAM-based optical interconnect operating at 1310 nm without using optical amplifications. Results are presented for both directly modulated laser (DML)- and externally modulated laser (EML)-based links operating with 4- and 8-PAM signaling and carry bit rate of 56, 112, and 224 Gbps. Polarization-division multiplexing (PDM) technique is applied to the EML-based link to double the bit rate without degradation the transmission distance. Analytical expressions are derived to characterize the bit error rate (BER) floor and it dependence on the relative intensity noise (RIN) of the transmission laser source. Simulation results obtained using Optisystem software show that maximum distance of 45 and 37 km can be achieved for 4- and 8-PAM system, respectively, when 112 Gbps bit rate and 0 dBm transmitter launch power are used. These are to be compared with 40 and 28 km, respectively, for 224 Gbps data rate.

Keywords Intensity modulation/direct detection (IM/DD), Optical pulse amplitude modulation (PAM), Data center optical interconnects

1. Introduction

Optical fiber links attract increasing interest for high-bit rate inter- and intra-connects for advanced data centers [1-5]. These links apply the main features and advantages of optical fiber communication for short-reach applications [6-8]. Further, the capacity of these links can be enhanced using different multiplexing techniques such as wavelength-division multiplexing (WDM) [3], [9-12], optical orthogonal frequency-division multiplexing (O-OFDM) [13-20], space-division multiplexing (SDM) [21-25], and hybrid multiplexing [26-29]. Low cost optical interconnects usually implemented using direct-detection (DD) optical receivers [30-33]. This type of receivers uses a photodiode, for optical-to-electrical conversion, followed by an electrical receiver. The DD receiver is considered cheaper than coherent optical receivers since it does not use a local laser acting as a local oscillator to be synchronized with the transmitter laser [34-36]. Further, DD receivers work efficiently with optical pulse amplitude modulation (PAM) signaling where the information is encoded on the intensity of the transmitted pulses [37-40]. Again, the intensity modulation (IM)-based optical transmitter is cheaper as compared with coherent optical transmitter. The intensity modulation can be achieved using directly modulated laser (DML) [41-45] or external intensity modulator (EIM) [46], [47]. Advanced in photonic and optoelectronic technology leads to design DML and EIM operating at bit rates above 100 Gbps [48-50].

Optical interconnects operating at 100 Gbps [51-54] and 400 Gbps [55-62] have attracted significant research efforts and standardization activities, such as the IEEE 802.3bs 400 Gbps Ethernet Task Force [62]. These links are expected to play key role in data centers and short-reach communication. An active research topic in this field is to design low-cost version of optical interconnect based mainly on IM/DD system adopting advanced modulation formats and to enhance the operating rate above 400 Gbps. One of the modulation formats which drawn significant attraction for optical interconnect is multilevel PAM which can be incorporated easily in IM/DD system and it is free of digital-to-analog converter [63-67]. Further, it can be implemented using DML which highly preferred due its low cost and simple implementation. These features have encouraged different research groups to demonstrate successfully 4- and 8-PAM optical interconnects for data centers and short reach applications at 1550 nm wavelength [5], [68-69]. These experiments have been demonstrated using multimode fibers or single mode fiber SMFs and DMLs or EIMs. The 112 Gbps bit rate has been achieved using 4-PAM [70] and 8-PAM [19] signaling. Higher bit

* Corresponding author:
duhasabah94@gmail.com (Duha S. Ahmed)
Published online at http://journal.sapub.org/ijnc

rates can be achieved by applying wavelength-division-multiplexing techniques [11], [71].

Recently, there is interest to investigate 1310 nm-optical links for data centers. The negligible chromatic dispersion of the SMF at this wavelength enables higher bit rate transmission distance product compared with 1550 nm link and this can be achieved without using any dispersion compensation techniques which are usually adopted in 1550 nm links. In 2017, Miao et al. [72] developed scalable and fast optical switching system for 1310 nm optical interconnect carrying 4×25 Gbps, 4-PAM signals. Mosman et al. [73] demonstrated the transmission of polarization-division-multiplexing (PDM) 224 Gbps 4-PAM signals at 1310 nm over 10 km SMF using a single IM laser and DD multi-input multi-output (MIMO) DSP-based receiver. A 140 Gbps 20 km transmission of 4-PAM signal at 1310 nm has been demonstrated by Zhong et al. using externally modulated laser [74]. It is clear from the above survey that most research concerned with amplified 1550 nm PAM link where optical amplifier is used to boost the launch power and/or to compensate fiber loss.

The aim of this paper is to investigate the transmission performance of an unamplified 1310 nm optical interconnect. The interconnect is designed without using optical amplifiers which reduces the cost and increases the robustness of the link. The bit error rate (BER) characteristics of the DD receiver is analyzed for both 4-PAM and 8-PAM signals. Analytical expression is derived to describe the dependence BERfloor level on laser relative intensity noise (RIN) and other system parameters. Results are presented for 56, 112, and 224 Gbps PAM system using DML and external modulated laser (EML). The effect of applying PDM on the EML-link to double the transmission bit rate is also investigated. The transmission performance of the investigated PAM systems is obtained by simulating them using Optiwave software package ver.15.

2. Performance of DML and EIM-Interconnects

This section presents results characterize the transmission performance of data center optical interconnect based on PAM modulation. The results are reported for unamplified links operating at 1310nm wavelength with 56, 112, and 224 Gbps data rates using 4- and 8-PAM signaling are adopted at the transmitter using either DML or external modulator while the receiver uses a PIN direct detection configuration. The maximum transmission distance is estimated at BER threshold of 4.4 $\times 10^{-3}$ which corresponds to 7% over head hard decision (HD)-forward error correction (FEC) code. This BER threshold yields a 10^{-15} BER after applying the HD-FEC coder. Unless otherwise stated, the parameters values used in the calculations and simulation are listed in Table 1.

Table 1. Parameters values used in the simulation

Subsystem	Component	Parameters	Values
Optical Transmitter	Directly Modulated Laser (DML)	Wavelength	1310 nm
		Launch Power	0 dBm
Optical Link	Fiber (SMF)	Attenuation	0.35 dB/km
		Dispersion	0
		Dispersion Slope	0.092 Ps/nm^2. km
Optical Receiver	PIN Photodetector	Responsivity	1 A/W
		Thermal Power Density	10^{-22} W/Hz
		Load Resistance	550 Ω
	Receiver LPF	Cut off Frequency	0.75 × Sampling Rate

2.1. Directly Modulated Laser-Based Link

2.1.1. System under Investigation

Figure. 1 shows the DML-based system under investigation. The M-PAM generator is driven by the input binary data, after converting them a M-PAM sequence using the PAM encoder and generates equal-space radio frequency (RF) PAM signal. This signal is used as the drive current for the DML. For M-PAM signaling, the laser drive current takes the following form

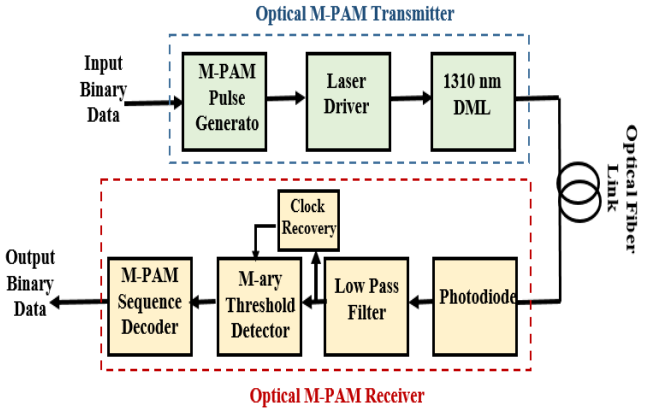

Figure 1. Overview block diagram of unamplified M-PAM single-channel system

$$I_i = I_{min} + m\,\Delta I \quad 0 \le m \le M\text{-}1 \qquad (1)$$

Where I_{min} corresponds to m=0 level and ΔI denotes level spacing. The maximum rate of PAM drive current $I_{max} = I_{min} + (M-1)\Delta I$. The average value of the drive

current (under the assumption of equal-probability symbols) is given by

$$I_{av} = \frac{I_{max}+I_{min}}{2} = I_{min} + \frac{(M-1)\,\Delta I}{2} \quad (2)$$

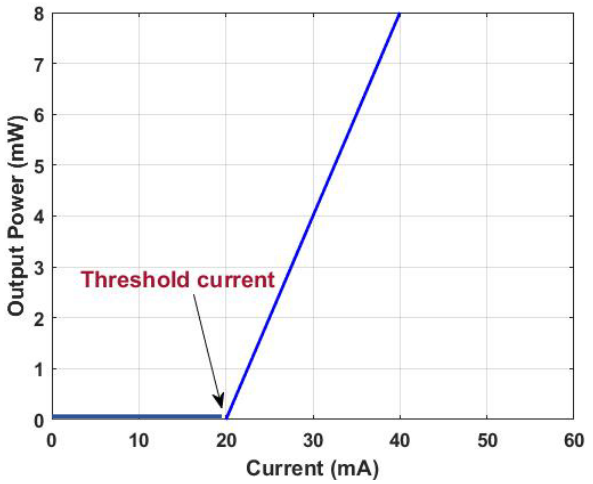

(a)

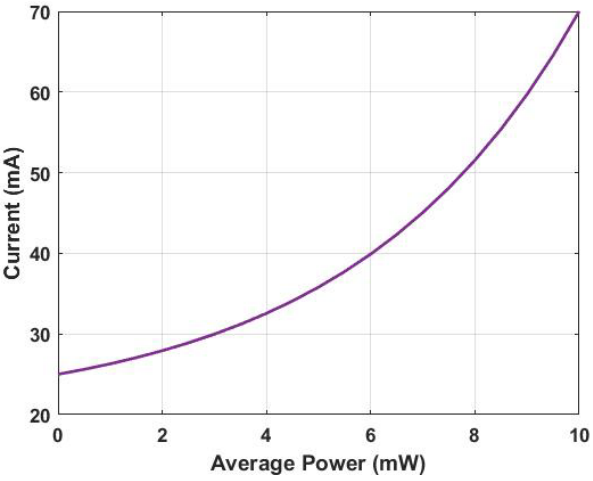

(b)

Figure 2. Laser diode static characteristics (a) power-current characteristics (b) calculated maximum drive current required to achieve a given average emitted power

To increase the switching spaced of the DML, the OFF state corresponding to I_{min} is obtained by setting I_{min} slightly above laser threshold current so the laser is ready to switch quickly to one of the ON states. In this subsection, the semiconductor laser used in the simulation is characterized by a 20 mA-threshold current I_{th} with a linear power-current characteristics in the lasing region

$$P = \eta_s(I - I_{th}) \text{ where } I \geq I_{th} \quad (3)$$

where P is the optical power emitted from the laser diode (LD) when driven by a current I and η_S is the slope efficiency which is set to 0.4 mW/mA in the simulation. Under the assumption that $I_{min} \geq I_{th}$, the average power P_{av} emitted from the laser is given by

$$P_{av} = \eta_s[I_{min} - I_{th} + \frac{M-1}{2}\Delta I] \quad (4a)$$

or

$$P_{av} = \eta_s[\frac{I_{max}+I_{min}}{2} - I_{th}] \quad (4b)$$

The required I_{max} to achieve a specific level of P_{av} is then given by

$$I_{max} = \frac{2P_{av}}{\eta_s} + 2I_{th} - I_{min} \quad (5)$$

$$I_{max} = \frac{2P_{av}}{\eta_s} + I_{th} \text{ where } I_{min} = I_{th} \quad (6)$$

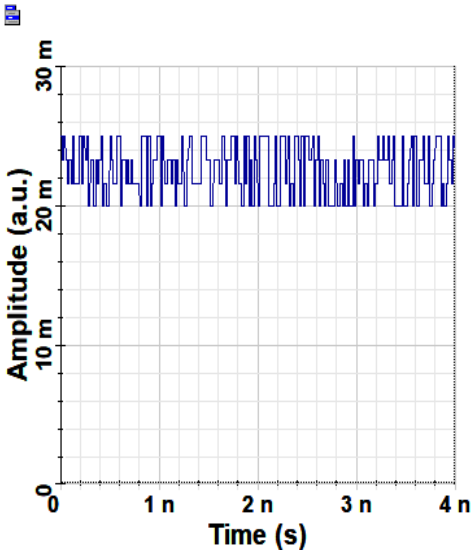

(a)

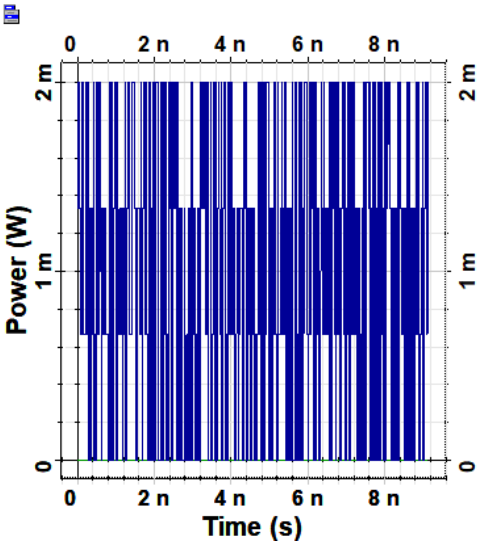

(b)

Figure 3. Waveforms for 112 Gbps 4-PAM corresponding to 0 dBm average power (a) drive current waveform (b) emitted optical waveform

The results are presents here for $I_{min} = I_{th}$ and therefore, the emitted optical power P corresponds to the zero-order level (m=0) equals zero. Figure 2a shows that the power-current characteristics of the LD used in the simulation while Figure 2b displays the calculated maximum drive current required to achieve a given average emitted power. The drive current waveform and the corresponding emitted optical waveform

are depicted in Figures 3a and 3b, respectively, for 112 Gbps 4-PAM corresponding to 0 dBm average power. Corresponding results related to 8-PAM system are given in Figures 4a and 4b.

The optical receivers incorporate a clock recovery circuit which is very essential in practical system to track any variation in the transmitted symbol rate. Further, a multi threshold circuit is adopted at the receiver to estimate the transmitted symbol level under observation which then be converted to a binary sequence using PAM decoder.

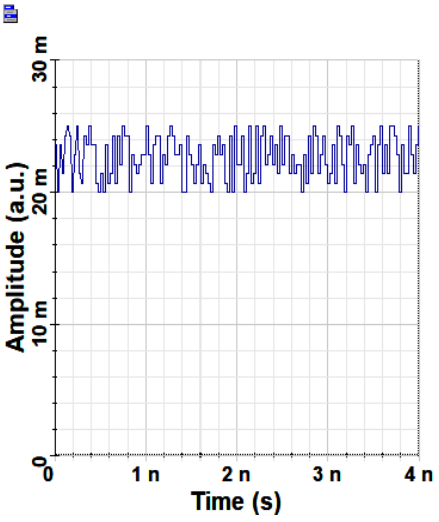

(a)

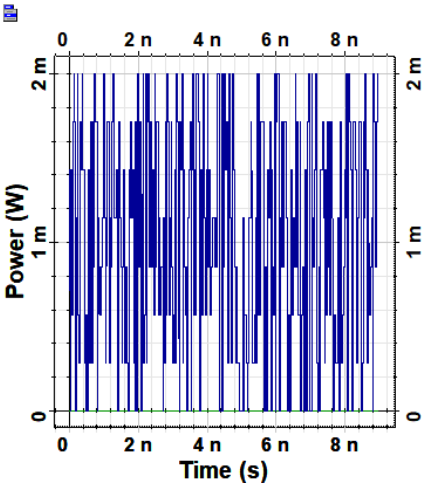

(b)

Figure 4. Waveforms for 112 Gbps 8-PAM corresponding to 0 dBm average power (a) drive current waveform (b) emitted optical waveform

2.1.2. Transmission Performance

Figure 5 shows the spectrum of the waveform at different points of the link for 112 Gbps 4-PAM system operating with 0 dBm launch power (average power at the fiber input) and 50 km transmission distance. Note that the spectrum of the RF PAM signal is copied on the upper and lower sidebands of the optical carrier. Note further that spectrum of the filtered photogenerated signal is confined within 42 GHz corresponding to 0.75 (R_S/2) which is the receiver electrical bandwidth. The received eye diagrams corresponding to different lengths are given in Figure 6. The results are given for transmission lengths L=0 (back-to-back (B2B)), 20, 40, and 60 km. The BER are 0, 0, 9.7×10^{-4} and 2.3×10^{-1}, respectively. The eye diagram corresponding to maximum reach L_{max} = 45 km is given in part e of this figure.

The simulation in Figures 5 and 6 are repeated for 8-PAM system operating with 112 Gbps bit rate and the results are given in Figures 7 and 8. Note that the spectrum of the filtered photogenerated signal in this case equals to 28 GHz corresponding to 0.75 (R_S/2). The maximum reach equals to 37 km for this link. The simulation in Figures 5 and 6 are repeated for 8-PAM system operating with 112 Gbps bit rate and the results are given in Figures 7 and 8. Note that the spectrum of the filtered photogenerated signal in this case equals 28 GHz corresponding to 0.75 (R_S/2). The maximum reach equals 37 km for this link.

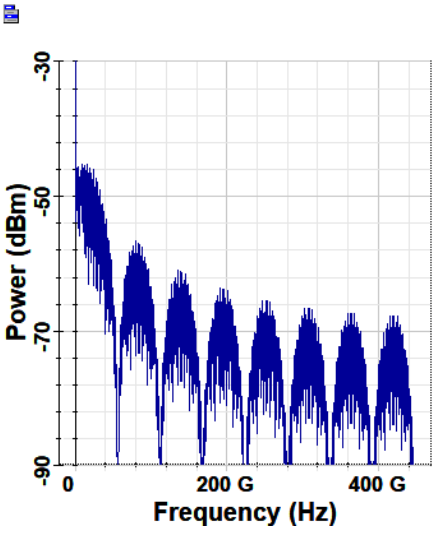

(a)

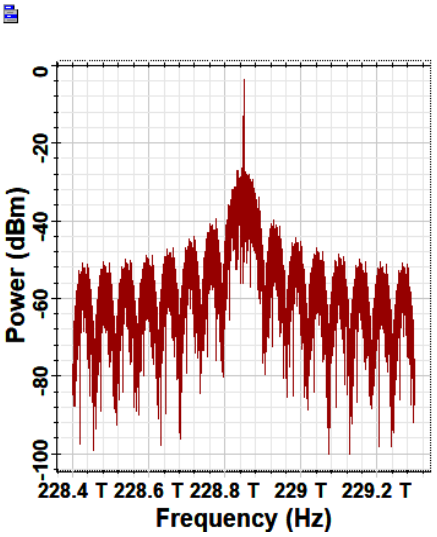

(b)

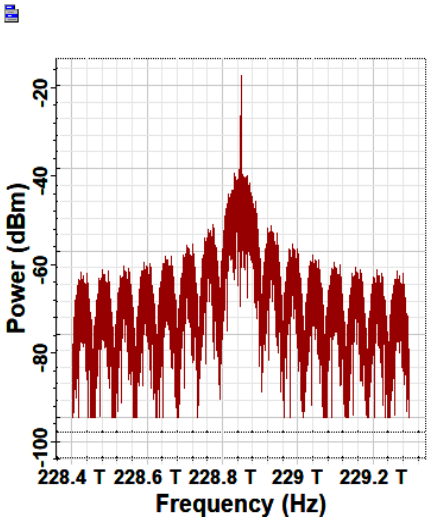

(c)

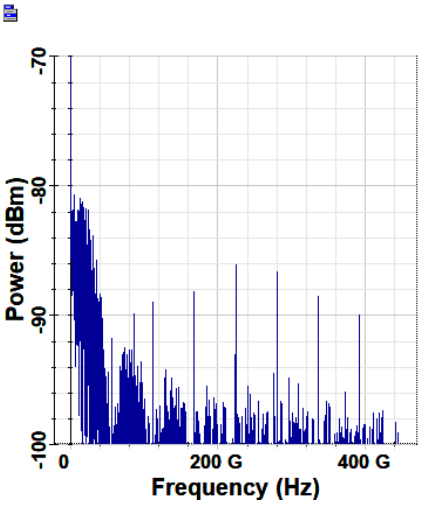

(d)

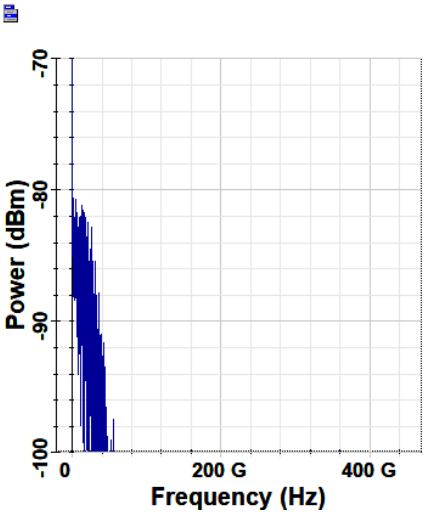

(e)

Figure 5. Spectra of the waveforms at different points of 50 km-link assuming 112 Gbps 4-PAM signaling with 0 dBm launch power (a) RF spectrum at the transmitter (b) optical spectrum after DML (c) optical spectrum at the receiver input (d) RF spectrum of the photogenerated current (e) RF spectrum after receiver LPF

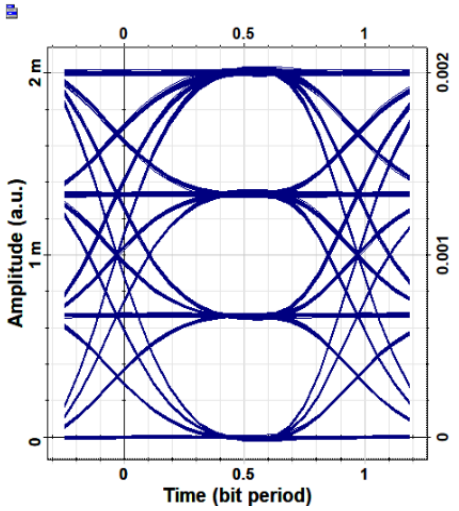

(a)

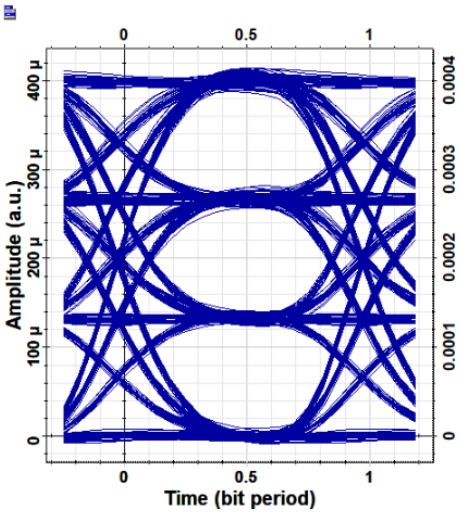

(b)

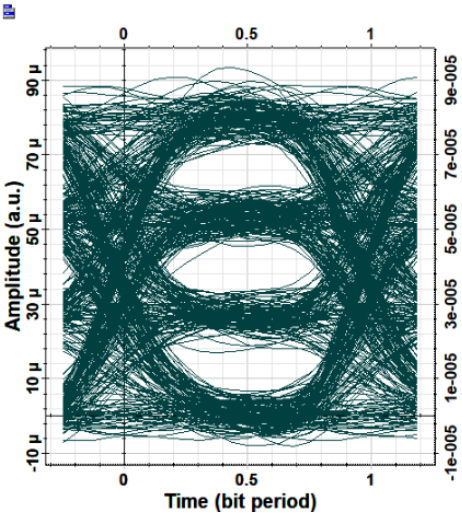

(c)

Figure 6. Receiver eye diagrams at 0 dBm launch power and for different lengths of 112 Gbps 4-PAM link (a) B2B (b) 20 km (c) 40 km (d) 60 km (e) 45 km maximum reach

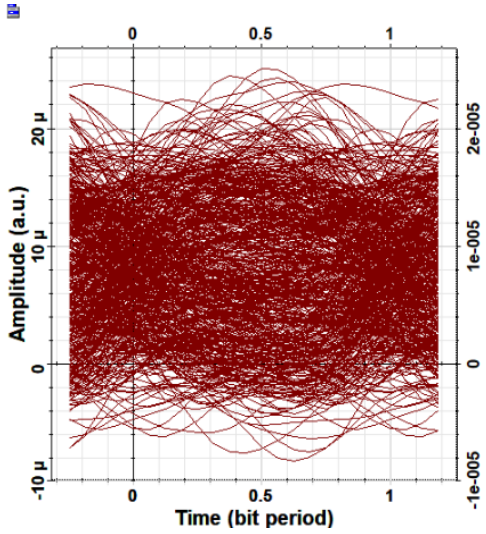

(d)

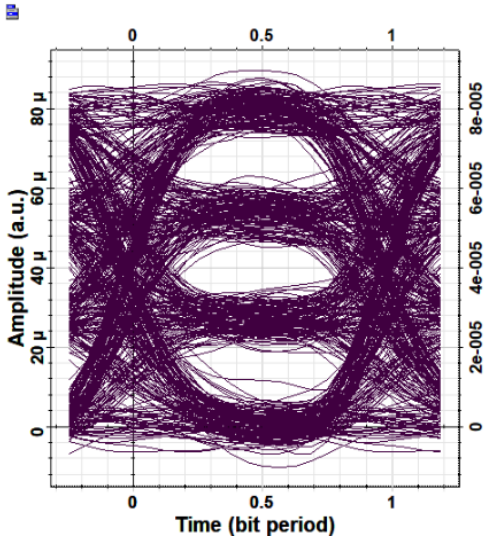

(e)

Figure 6. (Continued)

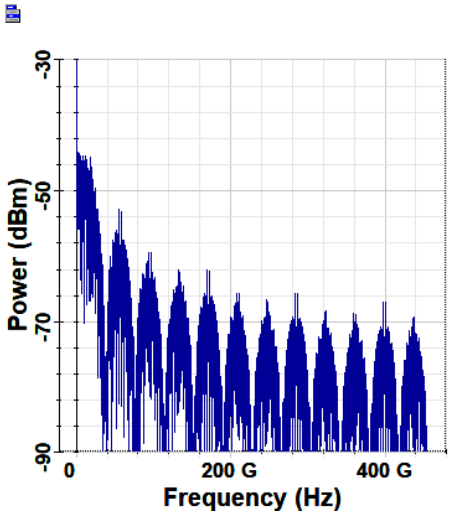

(a)

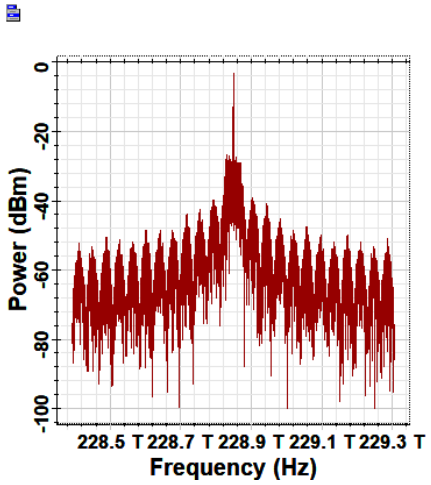

(b)

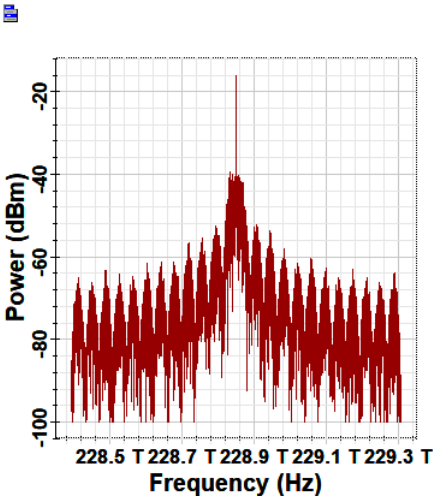

(c)

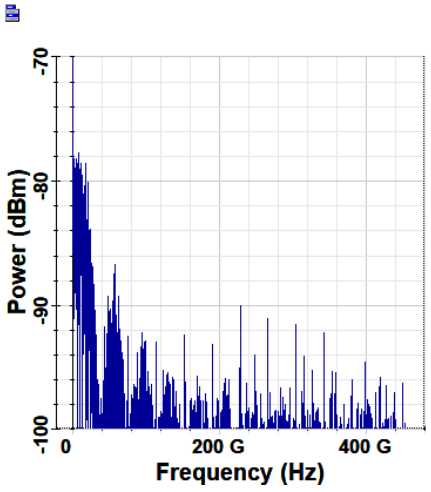

(d)

Figure 7. Spectra of the waveforms at different points of 50 km-link assuming 112 Gbps 8-PAM signaling with 0 dBm launch power (a) RF spectrum at the transmitter (b) optical spectrum after DML (c) optical spectrum at the receiver input (d) RF spectrum of the photogenerated current (e) RF spectrum after receiver LPF

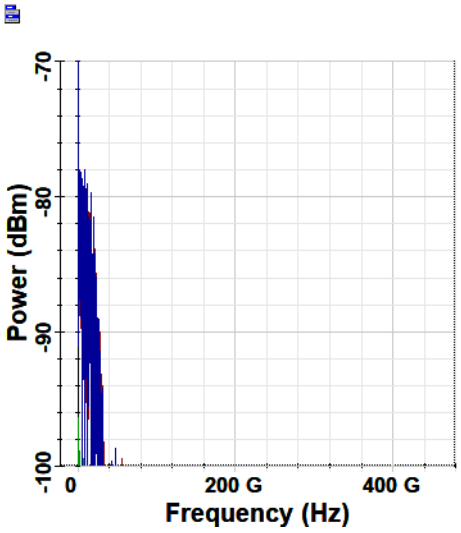

(e)

Figure 7. (Continued)

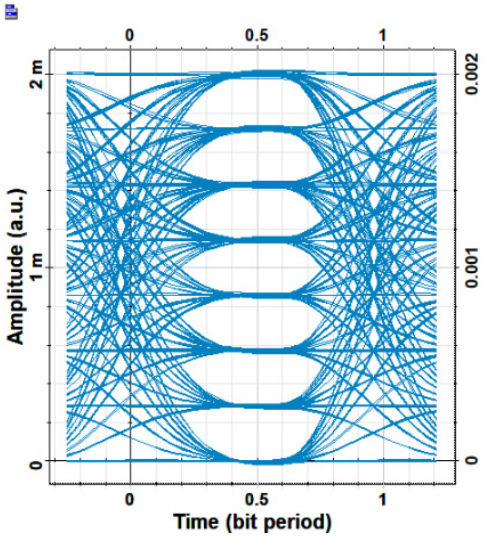

(a)

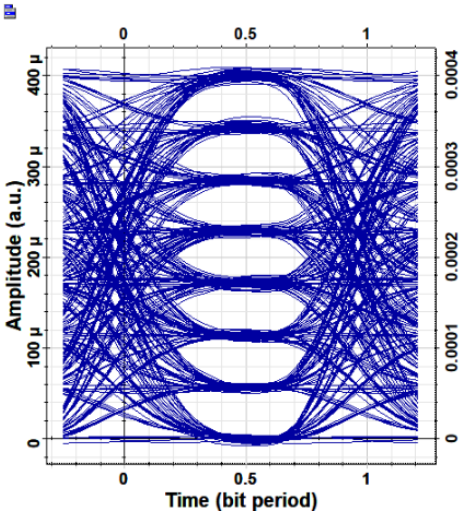

(b)

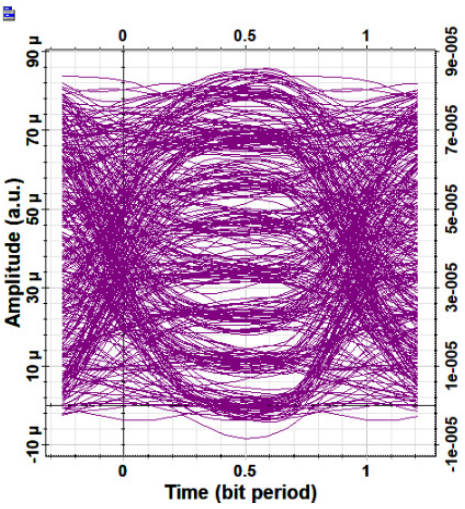

(c)

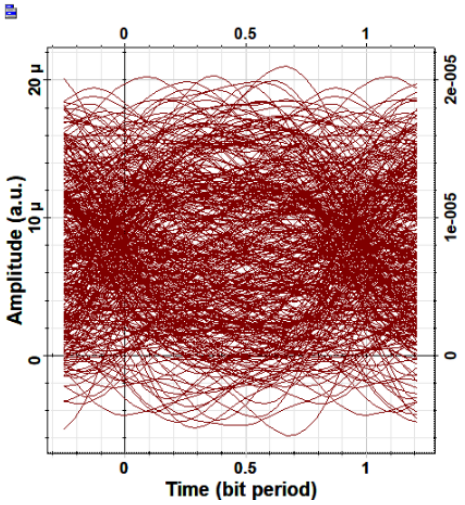

(d)

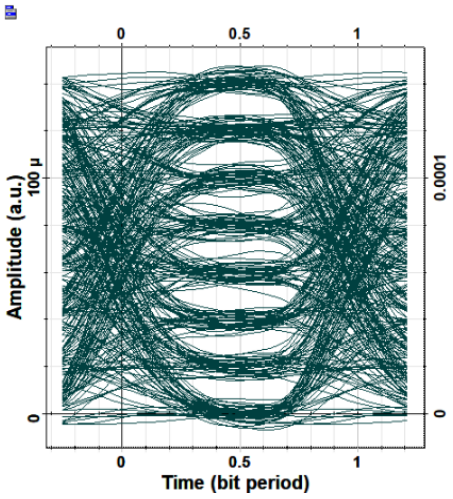

(e)

Figure 8. Receiver eye diagrams at 0 dBm launch power and for different lengths of 112 Gbps 8-PAM link (a) B2B (b) 20 km (c) 40 km (d) 60 km (e) 37 km maximum reach

The maximum reach L_{max} is investigated for both 4- and 8-PAM links operating with 56, 112, and 224 Gbps. At $L=L_{max}$ the BER approaches the threshold level (4.4×10^{-3}). The variation of BER with transmission distance is given in Figures 9a and 9b for 4- and 8-PAM link, respectively. The results are presented for 0 dBm transmitted power and indicate that L_{max} = 49, 45, and 37 km for 4-PAM link operates with bit rate R_b of 56, 112, and 224 Gbps, respectively. These values are to be compared with L_{max} = 42, 37, and 28 km respectively, for the 8-PAM links.

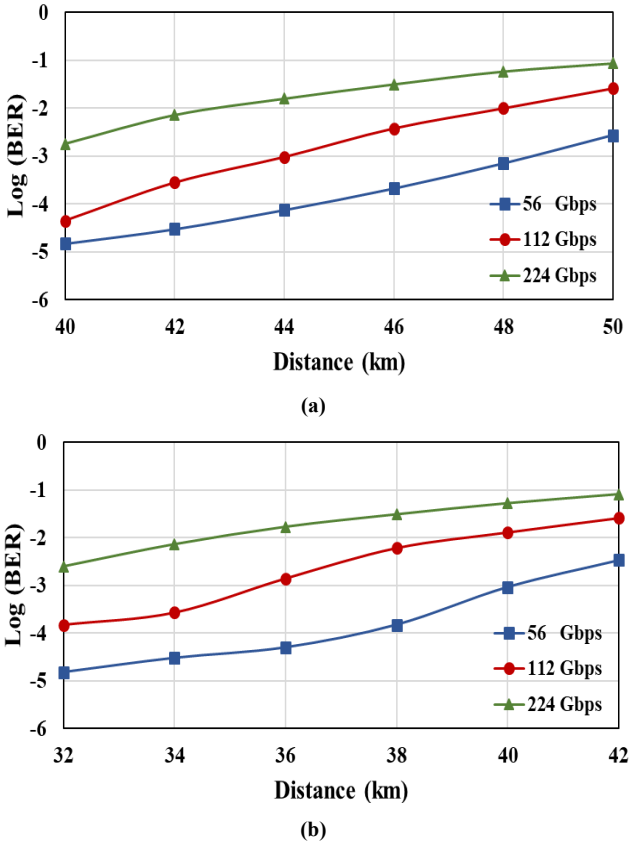

Figure 9. Variation of BER with transmission distance for (a) 4-PAM link (b) 8-PAM link. The results are presented for 0 dBm transmitted power

The dependence of BER on the launch power at fixed transmission length is depicted in Figures 10a and 10b for 45 km 4-PAM and 37 km 8-PAM links, respectively. The results are given for 56, 112, and 224 Gbps. Note that minimum launch power $(P_T)_{min}$ required to achieve the BER threshold equals -2, 0, and 2 dBm for the 4-PAM link when operates with 56, 112, and 224 bit rate, respectively. The corresponding results for the 8-PAM link is -1, 0, and 2 dBm, respectively.

The dependence of maximum reach L_{max} on the transmitter launch power P_T is deduced by simulating the system for each value of P_T and taking the transmission distance as the independent parameter. The results are displayed in Figures 11a and 11b for 4- and 8-PAM link, respectively. The values of L_{max} are estimated for three-bit rates, 56, 112, and 224 Gbps investigating the results in Figures 11a and 11b reveals the following findings.

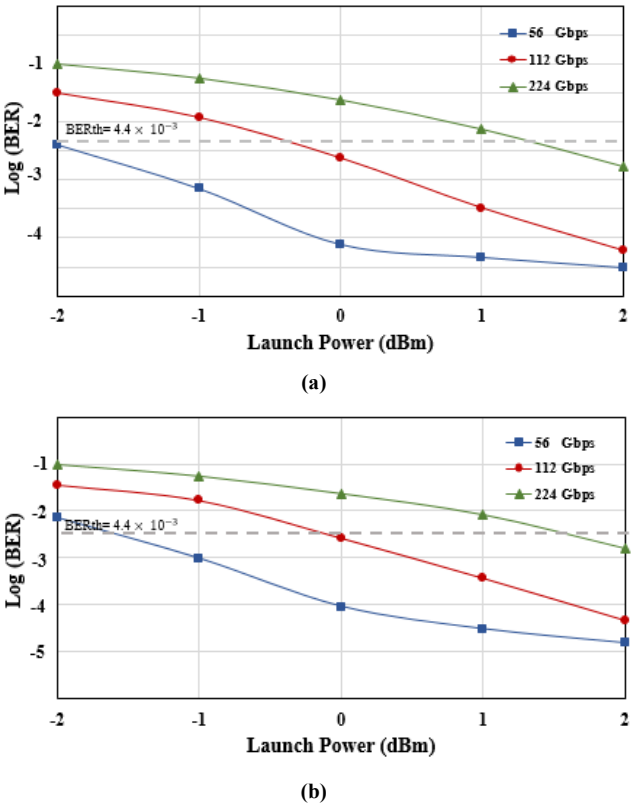

Figure 10. Dependence of BER on launch power at fixed transmission length (a) 45 km 4-PAM link (b) 37 km 8-PAM link

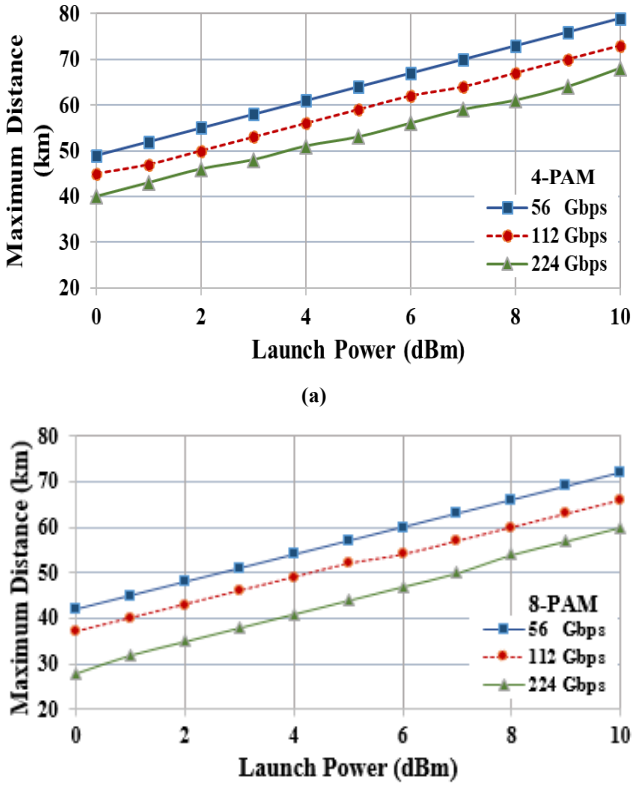

Figure 11. Maximum distance versus launch power (a) 4-PAM (b) 8-PAM

The maximum transmission distance in km is varied almost linearly with transmitter launch power (measured in dBm) with slope equals approximately to 2.9 km/dBm. This fact is true for both links and for the three bit rates. Note that the slope corresponds to 1/fiber loss (0.35/km used in the simulation) and indicate clearly that the system performance is loss limited.

(i) The L_{max}-P_T curves can be approximated by the linear relation $L_{max} = L_{max0} + 2.9\ P_T$ (dBm), where L_{max0} corresponds to L_{max} deduced at $P_T = 0$ dBm. The values of Lmax0 equal to 49, 45 and 40 km for 4-PAM link operating with R_b= 56, 112, and 224 Gbps. These values are to be compared with L_{max0} = 42, 37 and 28 km for the 8-PAM link, respectively.

(ii) At given launch power, increasing the bit rate from 56 Gbps to 112 Gbps and from 56 Gbps to 224 Gbps will reduce the maximum reach by 4 and 8 km, respectively for the 4-PAM link. Similarly, the maximum reach reduces by 5 and 9 km for the 8-PAM link for the same increase in the data rate. For examples at P_T = 2 dBm, L_{max} = 55, 50, and 46 km for the 4-PAM and 48, 43, and 35 km for the 8-PAM when the R_b = 56, 112, and 224 Gbps, respectively.

(iii) For given bit rate and launch power, the 4-PAM link offers longer transmission reach compared with the 8-PAM counterpart. At P_T = 2 dBm, $\Delta L_{max} = (L_{max})_{4\text{-PAM}} - (L_{max})_{8\text{-PAM}}$ equals to 7, 7, and 11 km for 56, 112, and 224 Gbps bit rate, respectively. These values of ΔL_{max} are almost independent of P_T.

2.2. External Intensity Modulator-Based Link

In this subsection, the transmission performance of the EIM PAM link is investigated. Results are presented for both single- and dual- polarization EIM-based configurations.

2.2.1. Single-Polarization EIM Link

Figure 12 show a simplified block diagram used in this simulation. A semiconductor laser operating in continuous-wave (CW) mode is used whose output is applied to the EIM. The electrical PAM signal X_{PAM} (t) is also applied to the modulator and acts as a modulating signal for the CW optical power. Ideally, the modulator yields an optical PAM signal P_{PAM} (t) = X_{PAM} (t).P_{CW} where P_{CW} presents the CW laser power. Under this ideal condition, the average power of the optical PAM signal $P_T = 0.5P_{CW}$ which corresponds to 3 dB loss. Figures 13a and 13b shows the waveform of the PAM signal at the modulator output for 112 Gbps 4- and 8-level system, respectively, when P_{CW} = 3 dBm.

Figure 14 shows the variation of maximum reach with CW laser power P_{CW} for the 4-PAM link. The results are presented for three values of bit rates 56, 112, and 224 Gbps. The values of Lmax is almost identical to those obtained with DML link operating with launch power $P_T = 0.5P_{CW}$. This conclusion is expected since the average power at the fiber input is identical in both cases under these power condition.

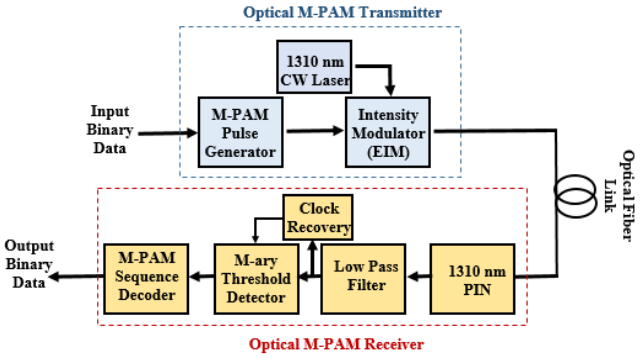

Figure 12. Overview block diagram of unamplified M-PAM single-channel system using EIM link

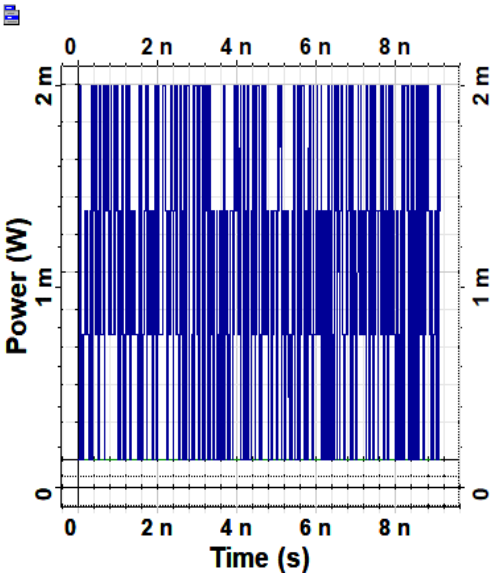

(a)

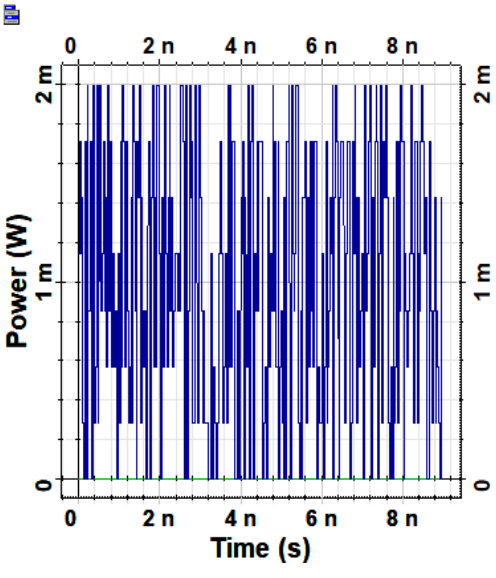

(b)

Figure 13. Waveforms of the PAM signals at the external modulator output for 112 Gbps link operating with PT = 0.5PCW (a) 4-PAM (b) 8-PAM

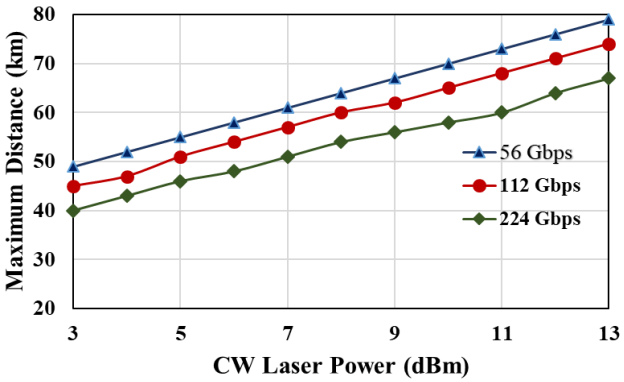

Figure 14. Maximum distance versus the CW laser power for 4-PAM EIM link

2.2.2. Dual-Polarization EIM Link

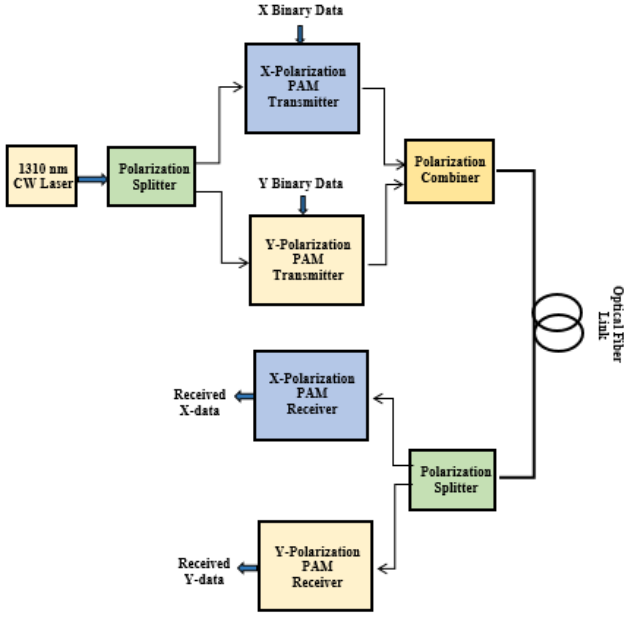

Figure 15. Overview block diagram of unamplified dual-polarization EIM 4-PAM system

The transmission bit rates of 112 and 224 Gbps using 4-PAM can be doubled in the EIM link if the system is re-configured using dual-polarization configuration (see Figure 15). The dual-polarization scheme can be considered as transmitting two PAM signals simultaneously over the link, each is carried by one of the two orthogonal polarization components of the optical field (X- and Y-polarization). In this configuration, the electrical field of the CW laser is adjusted into linearly-polarized state with polarization angle $\theta_P = 45°$ A polarization beam splitter is used then to split the CW laser power PCW into orthogonally polarized components: $P_X = P_{CW} \cos^2\theta_P$ and $P_Y = P_{CW} \sin^2\theta_P$ for $\theta_P = 45°$, $P_X = P_Y = 0.5P_{CW}$. Each polarization component acts as a CW optical carrier carrying half of the system bit rates. Under ideal conditions, the dual-polarization PAM link offer the same maximum reach as the single-polarization counterpart operating with half the bit rate and half the CW laser power. Eye diagrams results of X- and Y- polarization receivers of 4-PAM at maximum reach 45 and 39 km of bit rates 224 and 448 Gbps, respectively, 3 dBm CW laser power are shown in Figures 16. The maximum reach is investigated for 4-PAM link operating with bit rate 224 and 448 Gbps at different CW laser power and the results are shown in Figure 17.

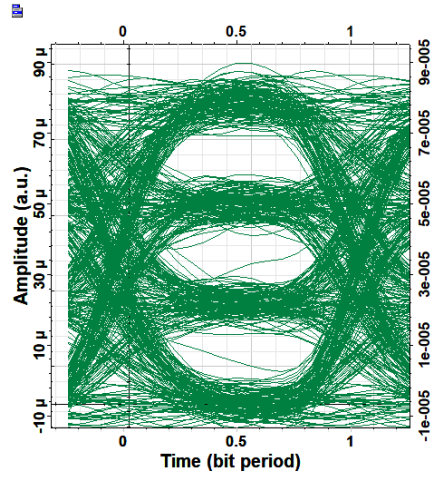

(a)

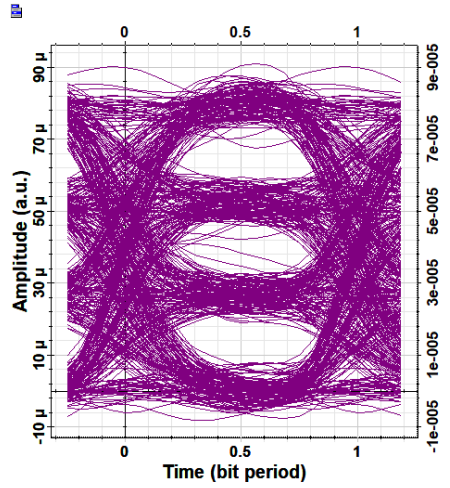

(b)

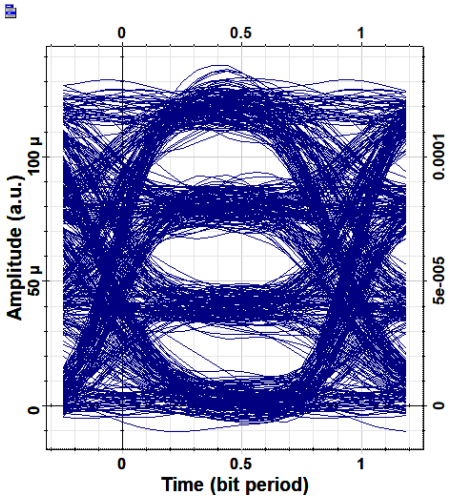

(c)

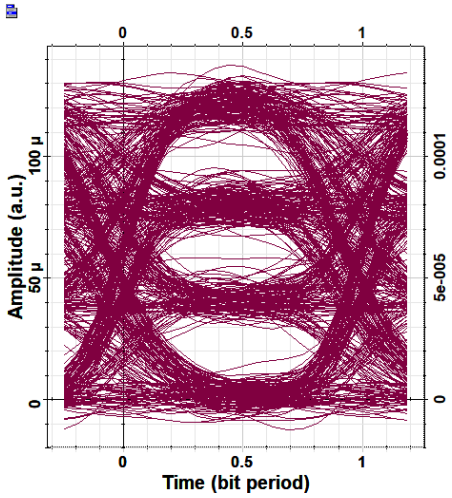

(d)

Figure 16. Receiver eye diagrams of dual polarization of 4-PAM (a) 224 Gbps X-polarization receiver (b) 224 Gbps Y-polarization receiver (c) 448 Gbps X-polarization receiver (d) 448 Gbps Y-polarization receiver. The results are obtained for P_{CW} = 3 dBm and maximum reach of 45 and 39 km for the 224 and 448 Gbps links, respectively

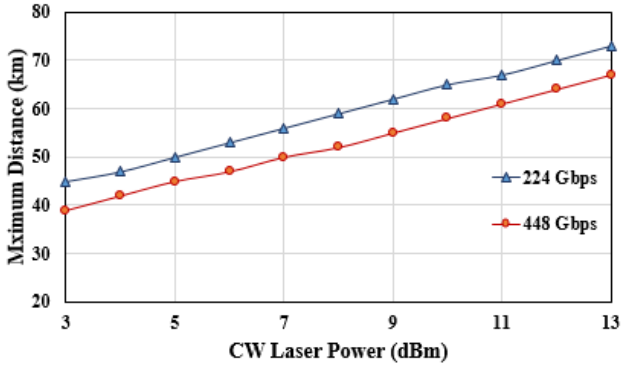

Figure 17. Maximum distance versus CW laser power for dual polarization EIM link

3. Noise and Bit Error Rate Characteristics

This section analysis the noise and bit error rate (BER) performance of 4- and 8-PAM link.

3.1. Bit Error Rate Formulation

BER of optical PAM communication system operating with unamplified transmission link and direct detection has been addressed by Szezorba et al. [75]. Their results show that when gray labelled M-PAM signaling is used with all the symbols have equal probability and equally speed, and the decision thresholds are equidistance from adjacent symbols, the BER can be expressed as [75].

$$BER = \frac{1}{Log_2 M}\left[\frac{M-1}{M}\, erfc\left(\frac{I_{Ph}}{\sqrt{2}(M-1)\sigma_t}\right)\right] \quad (7)$$

where I_{Ph} is the average photocurrent (i.e., average current generated by the photodiode) and σ_t denotes the standard deviation of the total noise current associated with the photo detection process (i.e., root-mean square (RMS) noise current). Further, erfc(.) represents the complementary error function of the argument. Note that the expression inside the square brackets describes the corresponding symbol error rate. Expressions corresponding to BERs of 2-, 4-, and 8-PAM systems can be deduced from eqn.7 and the results are

$$BER_2 = \frac{1}{2}\, erfc\left(\frac{I_{Ph}}{\sqrt{2}\sigma_t}\right) \quad (8a)$$

$$BER_4 = \frac{3}{8}\, erfc\left(\frac{I_{Ph}}{3\sqrt{2}\sigma_t}\right) \quad (8b)$$

$$BER_8 = \frac{7}{24}\, erfc\left(\frac{I_{Ph}}{7\sqrt{2}\sigma_t}\right) \quad (8c)$$

The average photocurrent I_{Ph} is related to the average received optical power P_r by

$$I_{Ph} = R_{Pd}\, P_r \quad (9a)$$

where R_{Pd} is the photodiode (PD) responsivity which de-scribes the optical-to-electrical conversion capability of the photodetection process and can be expressed as [75]

$$R_{Pd} = \frac{\eta_{Pd}\, q}{hf} = \frac{\eta_{Pd}\, q\lambda}{hc} \quad (9b)$$

where η_{Pd} is the quantum efficiency of the PD, q is the magnitude of the electronic charge, h = 6.6026×10^{-34} Js Planck's constant, and f = c/λ is the frequency of the incident optical signal with λ it's wavelength and c is the speed of light in free space.

The noise associated with the photodetection process comes mainly from three noise sources, namely thermal noise associated with the front-end electronic amplifier used to amplify the photocurrent, shot noise due to quantum nature of the photodetection, and relative intensity noise (RIN) which characterizes the intensity noise of the used transmitter laser. The variance of the total noise current can be written as

$$\sigma_t^2 = \sigma_{th}^2 + \sigma_{sh}^2 + \sigma_{RIN}^2 \quad (10)$$

where $\sigma_{th}^2, \sigma_{sh}^2$, and σ_{RIN}^2 are the variances corresponding to thermal noise, shot noise, and RIN, respectively, and they are calculated as follows [75]

$$\sigma_{th}^2 = \frac{4k_B T F_n B}{R_L} \quad (11a)$$

$$\sigma_{sh}^2 = 2q\, I_{Ph}\, B \quad (11b)$$

$$\sigma_{RIN}^2 = \text{RIN}\, I_{Ph}^2\, B \quad (11c)$$

where k_B = 1.381×10^{-23} J/k is Boltzman constant, T is the absolute temperature (in Kelvin), and B is the receiver electrical bandwidth. The receiver electronic amplifier is characterized by R_L load resistance and F_n noise figure. Few remarks related to eqns. 10 and 11 are given here

(i) The effect of the PD dark current shot noise (variance: $\sigma_d^2 = 2q\, I_d\, B$ with I_d is the dark current) is negligible compared with photocurrent shot noise σ_{sh}^2 and therefore σ_d^2 is not included in eqn. 10. This assumption is justified in practical receivers since $I_d << I_{Ph.}$

(ii) There are two signal-dependent noise sources,

namely photocurrent shot noise and RIN-related noise whose variances proportional to I_{Ph} and I^2_{Ph}, respectively. This implies that low-RIN laser sources should be used.

(iii) The receiver bandwidth B is related to the symbol rate $R_s = R_b/Log_2M$ where R_b is the bit rate. To ensure zero intersymbol interference (ISI) at the input of the receiver, $0.5R_s \leq B \leq R_s$ for the equalized pulse shape. Note that each of the noise variance scales linearly with symbol rate. At fixed bit rate R_b, going from 2-PAM to 4- and 8-PAM signaling will reduce the total noise σ_t^2 to half and third, respectively.

3.2. Noise and BER Results

This subsection presents noise and BER characteristics of the DD receiver used to recover the information from an optical PAM signal received after transmission over unamplified link. The system under investigation corresponds to a single-channel transmission at 1310 nm wavelength. The parameters values used in the simulation are listed in Table 1.

Figures 18a-d show the noise characteristics of 112 Gbps 4-PAM receiver, designed with 550 Ω amplifier load resistance RL and for four values of laser RIN, -130, -140, -150, and -160 dB/Hz, respectively. In these figures, the variance of the total noise σ_t^2 and variances of the individual noise sources ($\sigma_{th}^2, \sigma_{sh}^2$, and σ_{RIN}^2) are plotted in logarithmic scale versus the average received power Pr measured in dBm. The results are repeated in the Appendix for RL=50Ω. The 50 Ω load resistance corresponds to low impedance receiver front-end electronic amplifier which yields a 10^{-21} W/Hz thermal noise power spectral density (PSD) according to eqn. 11a. The 550 Ω load resistance corresponds to advanced receiver front-end electronic amplifier which has a transimpedance (feedback) configuration with 550 Ω feedback resistance. The feedback amplifier configuration offers the required bandwidth with higher value of resistance compared with low-impedance counterpart but with reduced thermal noise PSD = 10^{-22} W/Hz when 550 Ω resistance is used. Investigating these figures reveals that

(i) Both Log (σ_{sh}^2) and Log (σ_{RIN}^2) increase linearly with P_r (dBm) but with different slops which reflect the degree of dependence of these noise components on the photocurrent I_{Ph}. Recall that P_r (dBm)=10 Log [P_r (mW)] = 30 + 10 Log [P_r (W)], then eqns. 11b and 11c can be rewritten as

$$Log\ \sigma_{sh}^2 = -3 + Log(2qR_dB) + 0.1\ P_r(dBm) \quad (12a)$$

$$Log\ \sigma_{RIN}^2 = -6 + Log(R_d^2B) + 0.1RIN(dB/Hz) + 0.2\ P_r(dBm) \quad (12b)$$

Equations 12a and 12b indicate clearly that $Log\ \sigma_{sh}^2$ and $Log\ \sigma_{RIN}^2$ increases linearly $P_r(dBm)$ with slope equals 0.1 and 0.2, respectively.

(ii) The contribution of shot noise becomes higher than that of the thermal noise when the received optical power exceeds a certain level (denoted here by $(P_r)_{cross\text{-}shot}$). This P_r level equals to 5 and -5 dBm for the parameters values used in the simulation and when RL =50 Ω and 550 Ω, respectively. Generally, according to eqns. 11a and 11b

$$(P_r)_{cross-shot} = 2k_BTF_n/(qR_{Pd}R_L) \quad (13)$$

(iii) The contribution of RIN noise becomes higher than the contribution of the thermal noise when the received optical power exceeds a certain level $(P_r)_{cross\text{-}RIN}$ which depends on the level of RIN of the used optical source. Using eqns. 11a and 11c yields the following expression

$$(P_r)_{cross-RIN} = \frac{2}{R_{Pd}}\left(\frac{k_BTF_n}{RIN\ R_L}\right)^{1/2} \quad (14)$$

For the system under investigation, $(P_r)_{cross\text{-}RIN}$ equals -15, -10, -5, and 0 dBm for RIN = -130, -140, -150, and -160 dB/Hz, respectively when R_L equals 550 Ω. For 50 Ω-receiver, $(P_r)_{cross\text{-}RIN}$ equals -10, -5, 0, and 5 dBm for RIN = -130, -140, -150, and -160 dB/Hz, respectively.

(iv) Both $(P_r)_{cross\text{-}shot}$ and $(P_r)_{cross\text{-}RIN}$ are independent of symbol and bit rates.

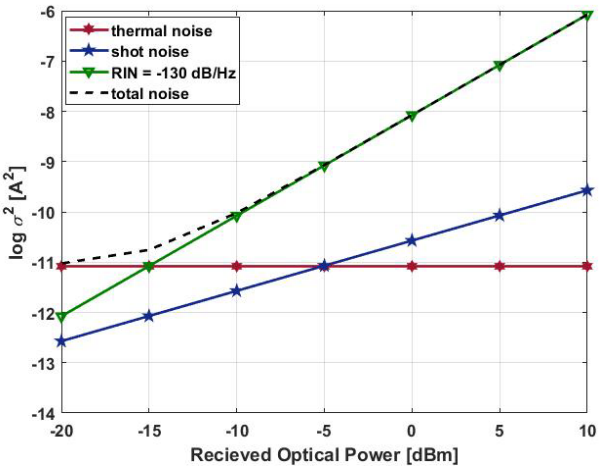

(a)

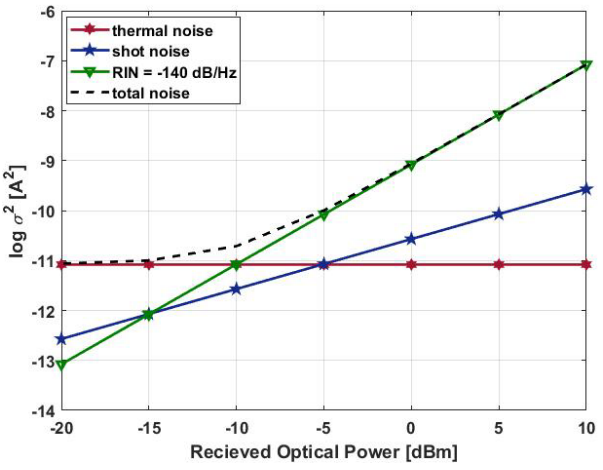

(b)

Figure 18. Noise characteristics of 112 Gbps 4-PAM receiver designed with 550Ω amplifier load resistance and for (a) RIN = -130 dB/Hz (b) RIN = -140 dB/Hz (c) RIN = -150 dB/Hz (d) RIN = -160 dB/Hz

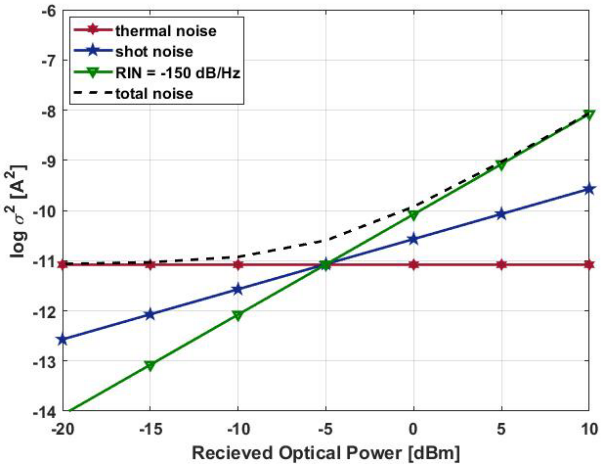

(c)

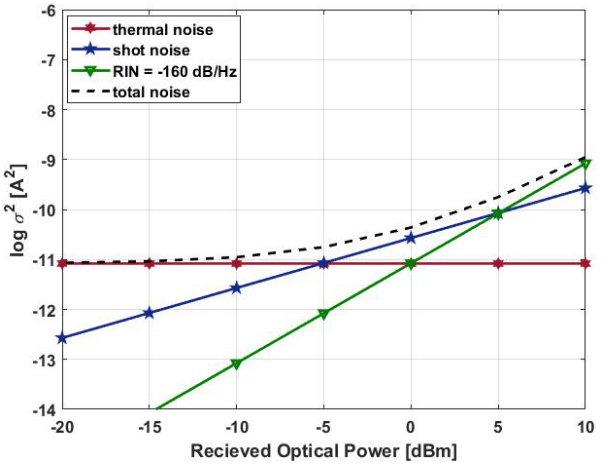

(d)

Figure 18. (Continued)

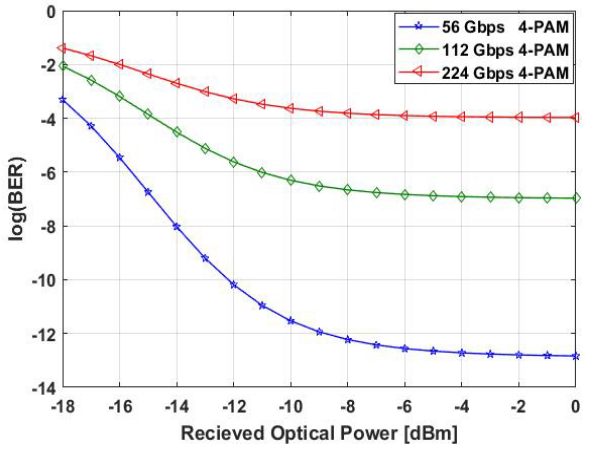

(a)

Figure 19. BER characteristics of the of 4-PAM optical receiver for (a) RIN = -130 dB/Hz (b) RIN = -140 dB/Hz (c) RIN = -150 dB/Hz (d) RIN = -160 dB/Hz

The BER characteristics of the optical PAM receiver is calculated using eqn.7 for 4- and 8-PAM signaling and the results are displayed in Figures 19 and 20, respectively. The results are presented for three values of bit rate (56, 112, and 224 Gbps) and four values of RIN (-130, -140, -150, and -160 dB/Hz). From these figures, one can construct Tables 2 and 3 which reflect the minimum values of average received power required to maintain BER less than 10^{-8} and 10^{-10}, respectively, for different system parameters. The minimum received optical power that yields the required BER level is called the receiver sensitivity. The mark (X) in these two tables denotes that this BER level cannot be reached.

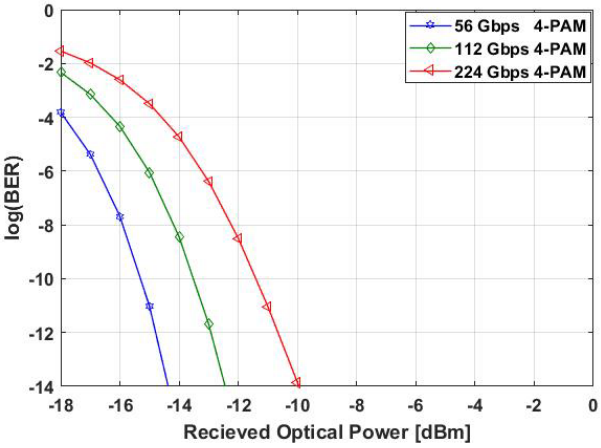

(b)

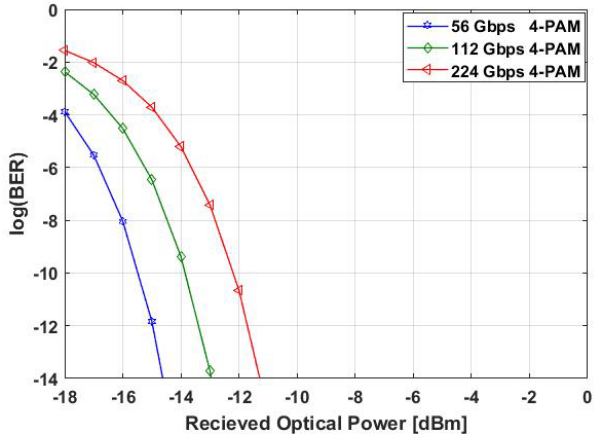

(c)

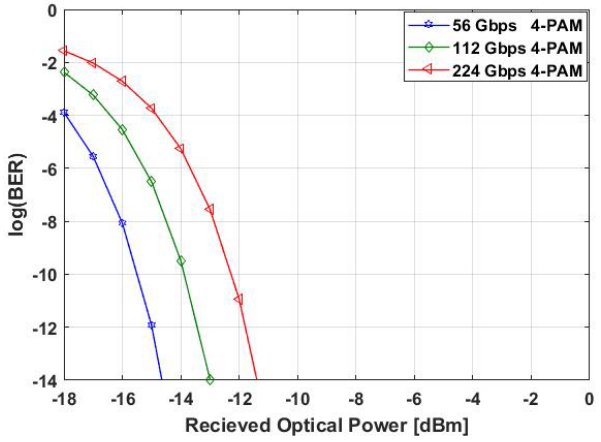

(d)

Figure 19. (Continued)

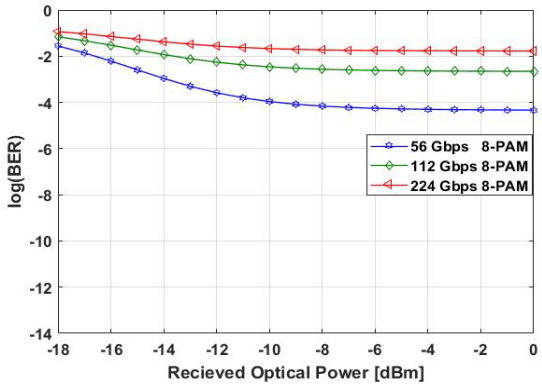

(a)

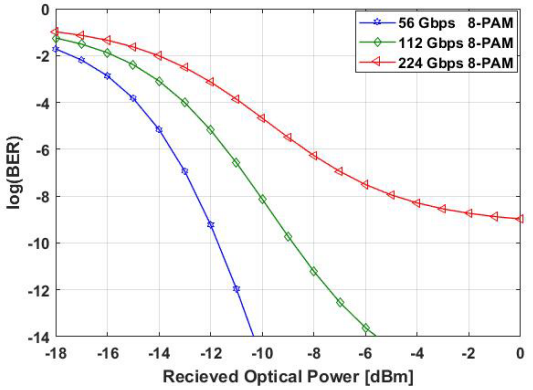

(b)

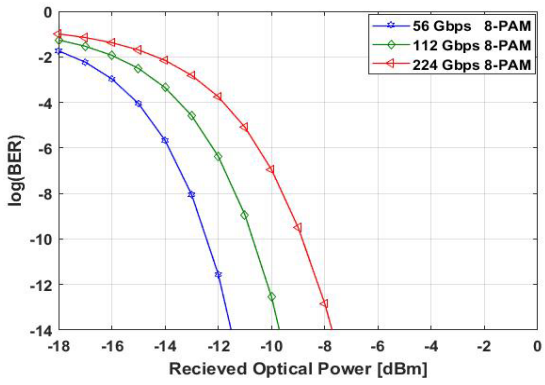

(c)

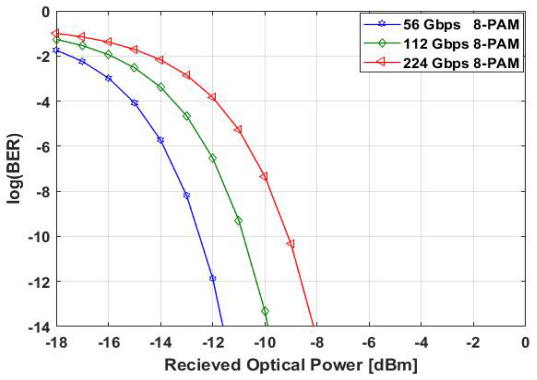

(d)

Figure 20. BER characteristics of the 8-PAM optical receiver for (a) RIN = -130 dB/Hz (b) RIN = -140 dB/Hz (c) RIN = -150 dB/Hz (d) RIN = -160 dB/Hz

Table 2. Sensitivity of 1310 nm PAM receiver for BER =10^{-8}. The mark "X" indicates that BER of 10-8 cannot be achieved under these conditions

(a) 4-PAM system

Bit rate (Gbps)	Receiver Sensitivity (dBm)			
	RIN -130 dB/Hz	RIN -140 dB/Hz	RIN -150 dB/Hz	RIN -160 dB/Hz
56	-14.0	-15.9	-16.0	-16.0
112	X	-14.2	-14.5	-14.5
224	X	-12.3	-12.8	-12.9

(b) 8-PAM system

Bit rate (Gbps)	Receiver Sensitivity (dBm)			
	RIN -130 dB/Hz	RIN -140 dB/Hz	RIN -150 dB/Hz	RIN -160 dB/Hz
56	X	-12.5	-13.0	-13.0
112	X	-10.1	-11.4	-11.5
224	X	-4.9	-9.5	-9.8

Table 3. Sensitivity of 1310 nm PAM receiver for BER =10^{-10}. The mark "X" indicates that BER of 10^{-10} cannot be achieved under these conditions

(a) 4-PAM system

Bit rate (Gbps)	Receiver Sensitivity (dBm)			
	RIN -130 dB/Hz	RIN -140 dB/Hz	RIN -150 dB/Hz	RIN -160 dB/Hz
56	-12.1	-15.2	-15.4	-15.5
112	X	-13.5	-13.9	-13.9
224	X	-11.4	-13.2	-13.2

(b) 8-PAM system

Bit rate (Gbps)	Receiver Sensitivity (dBm)			
	RIN -130 dB/Hz	RIN -140 dB/Hz	RIN -150 dB/Hz	RIN -160 dB/Hz
56	X	-11.8	-12.4	-12.5
112	X	-8.9	-10.9	-10.9
224	X	X	-8.9	-9.0

Note that at BER = 10^{-10} and RIN = -150 dB/Hz, the receiver sensitivity increases from -15.4 to -13.9 and -13.2 dBm when the R_b increases from 56 to 112 and 224 Gbps, respectively in the 4-PAM system. These values are to be compared with -12.4, -10.9, and -8.9 dBm receiver

sensitivity, respectively, for the 8-PAM system. Note further that increasing the RIN level may lead to BER-floor characteristics where the required BER cannot be achieved by increasing the received optical power. For example, the 4-PAM modulation does not yield a 10^{-8} BER for 112 and 224 Gbps bit rates when the RIN = -130 dB/Hz. The effect of RIN is more pronounced for the 8-PAM modulation. At RIN = -130 dB/Hz, the 10^{-8} BER cannot be achieved for the three values of bit rate used in the simulation.

3.3. BER-Floor Characteristics

The analysis is extended to address the BER-floor characteristics of the PAM receiver. It is clear from eqns. 7, 10 and 11, that the BER will saturate at certain level independent of received optical power P_r when the argument of the erfc in eqn.7 approaches a constant value independent of Pr. This occurs when the RIN noise dominates the receive noise. In this case $\sigma_t^2 = \sigma_{RIN}^2 =$ RIN $I_{Ph}^2 B$. From eqn.7, the BERfloor can be estimated as

$$BER_{floor} = \frac{1}{Log_2 M}\left[\frac{M-1}{M} erfc\left(\frac{1}{(M-1)\sqrt{2\,RIN\,B}}\right)\right] \quad (15)$$

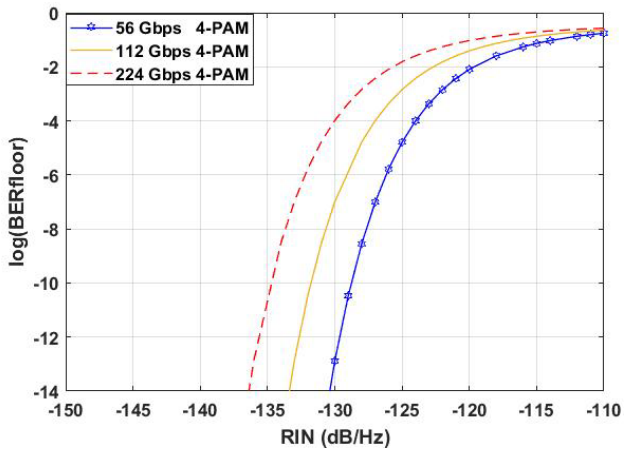

(a)

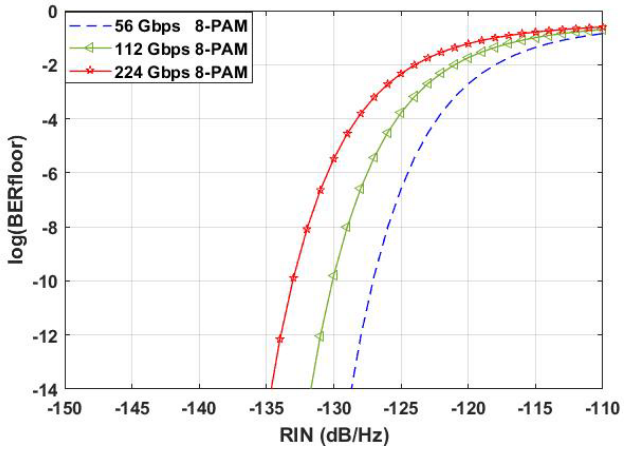

(b)

Figure 21. BER-floor as a function of RIN for (a) 4-PAM (b) 8-PAM

Equation 15 states that BERfloor increases with increasing bit rate and RIN level. This is demonstrated in Figures 21a and 21b where the BERfloor is calculated as a function of RIN for 4- and 8-PAM systems, respectively. To achieve a BER-floor less than 10^{-10} in the 4-PAM receiver, the RIN should be less than -125, -130 and -135 dB/Hz for R_b = 56, 112 and 224 Gbps, respectively. These values are to be compared with RIN = -125, -130 and -135 dB/Hz, respectively, when 8-PAM modulation is used.

The calculations are carried further to deduce the power penalty, Pen_{RIN}, due to the effect of using a laser source with non-negligible RIN. The penalty is defined as

$$Pen_{RIN} = \left|10\,Log\left(\frac{P_r(W)_{RIN}}{P_r(W)_{Ideal}}\right)\right|_{BER=constant} \quad (16a)$$

or

$$Pen_{RIN} = |P_r(dBm)_{RIN} - P_r(dBm)_{Ideal}|_{BER=constant} \quad (16b)$$

where the subscripts RIN and ideal are used to characterize a semiconductor laser having a finite RIN level and negligible RIN level, respectively. Table 4 lists the power penal-ty estimated at BER = 10^{-8} for both 4- and 8-PAM signaling.

Table 4. Power Penalty for BER = 10-10. The mark "X" indicates that BER of 10^{-10} cannot be achieved under these conditions

(a) 4-PAM system

Bit rate (Gbps)	Power Penalty (dBm)			
	RIN -130 dB/Hz	RIN -140 dB/Hz	RIN -150 dB/Hz	RIN -160 dB/Hz
56	4.15	1.05	0.85	0.75
112	X	0.5	0.1	0.1
224	X	3.3	1.5	1.5

(b) 8-PAM system

Bit rate (Gbps)	Power Penalty (dBm)			
	RIN -130 dB/Hz	RIN -140 dB/Hz	RIN -150 dB/Hz	RIN -160 dB/Hz
56	X	0.7	0.1	0.1
112	X	3.0	1.0	1.0
224	X	X	0.2	0.1

4. Conclusions

The noise characteristics and transmission performance of unamplified 1310 nm-optical link incorporating multilevel PAM signaling have been investigated when either DML or EML is used. Simulation results are presented for 56, 112, and 224 Gbps bit rates when 4- and 8-PAM are used without PDM technique. Applying PDM doubles the transmission bit rate of the EML-based link without affecting its maximum distance. The simulation

results reveal that using unamplified link based on 1310 nm SMF and supported by IM/DD scheme will offer robust and low-cost interconnect for data center which does not require dispersion-compensation scheme. For 0 dBm launch power, the maximum reach is 49, 45, and 40 km when 4-PAM link is used with bit rate 56, 112, and 224 Gbps, respectively, when PDM technique is not used. These values are to be compared with 42, 37, and 28 km, respectively, when 8-PAM is used. Further, a PDM 4-PAM system can support maximum reach of 45 and 39 km at 0 dBm laser power with 224 and 448 Gbps bit rate, respectively. The BER-floor characteristics of the PAM link has been also investigated analytically to address the effect of system parameters such as bit rate and RIN of the transmitter laser source. The investigation indicates that to achieve a BERfloor less than 10^{-10} in the 4-PAM receiver, the RIN should be less than -125, -130 and -135 dB/Hz for R_b = 56, 112 and 224 Gbps, respectively. These values are to be compared with RIN = -125, -130 and -135 dB/Hz, respectively, when 8-PAM modulation is used.

Appendix

Noise Components of 112Gbps 4-PAM Receiver Designed with 50Ω Loads Resistance

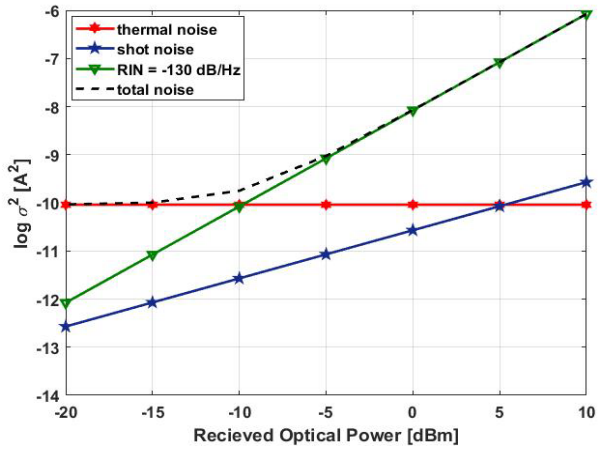

(a)

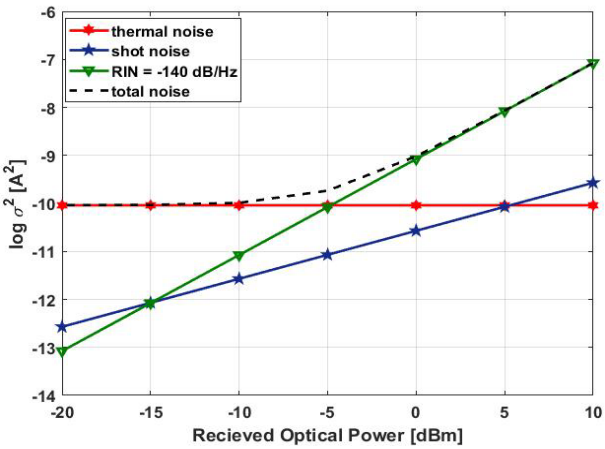

(b)

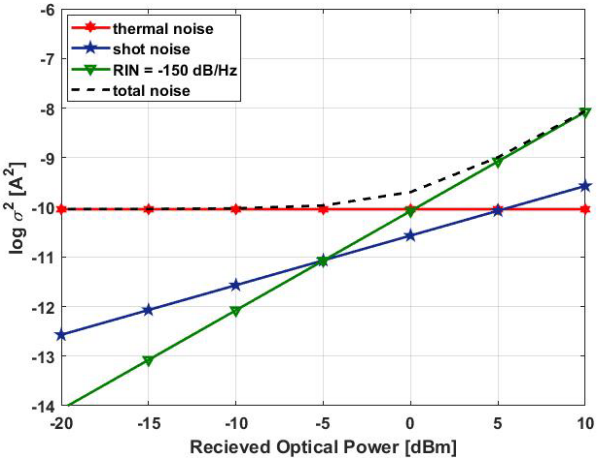

(c)

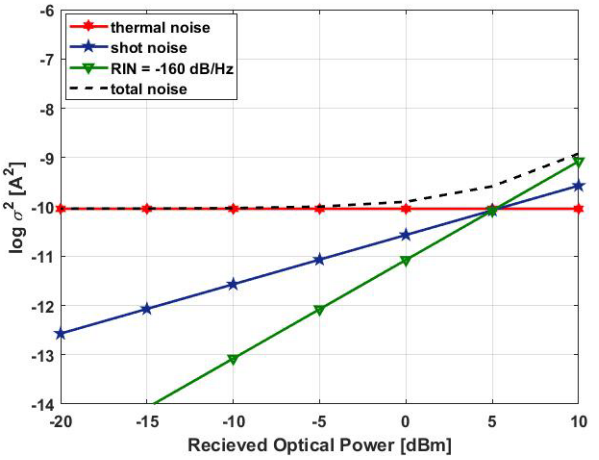

(d)

Figure 22. Noise characteristics of 112 Gbps 4-PAM receiver designed with 50Ω amplifier load resistance and for (a) RIN = -130 dB/Hz (b) RIN = -140 dB/Hz (c) RIN = -150 dB/Hz (d) RIN = -160 dB/Hz

REFERENCES

[1] C. Kachris and I. Tomkos, "A survey on optical interconnects for data centers," IEEE Communications Surveys and Tutorials, vol. 14, no. 4, pp. 1021-1036, Fourth Quarter 2012.

[2] G. Zervas, H. Yuan, A. Saljoghei, Q. Chen, and V. Mishra, "Optically disaggregated data centers with minimal remote memory latency: technologies, architectures, and resource al-location," Journal of Optical Communication and Networking, vol. 10, no. 2, pp. 270-285, Feb. 2018.

[3] S. K. Kang, J. Y. Huh, J. H. Lee, and J. K. Lee, " Low-cost and miniaturized 100-Gb/s (2 × 50 Gb/s) PAM-4 TO-packaged ROSA for data center networks," Optics Express, vol. 26, no. 5, pp. 6172-6181, Mar. 2018.

[4] D. Sadot, G. Dorman, A. Gorshtein, E. Sonkin, and O. Vi-dal1, "Single channel 112Gbit/sec PAM4 at 56Gbaud with digital signal processing for data centers applications," Optics Express, vol. 23, no. 2, pp. 991-997, Jan. 2015.

[5] E. El-Fiky, M. Chagnon, M. Sowailem, A. Samani, M. M.

Osman, and D. V. Plant, "168-Gb/s single carrier PAM4 transmission for intra-data center optical interconnects," IEEE Photonics Technology Letters, vol. 29, no. 3, pp. 314-317, Feb. 2017.

[6] M. M. Osman, M. Chagnon, M. Poulin, S. Lessard, and D. V. Plant, "224-Gb/s 10-km transmission of PDM PAM-4 at 1.3 μm using a single intensity-modulated laser and a direct-detection MIMO DSP-based receiver," IEEE Journal of Lightwave Technology, vol. 33, no. 7, pp. 1417-1424, Apr. 2015.

[7] M. R.T. Tan, P. Rosenberg, W. V. Sorin, B. Wang, S. Mathai, G. Panotopoulos, and G. Rankin, "Universal photonic inter-connect for data centers," IEEE Journal of Lightwave Technology, vol. 36, no. 2, pp. 175-180, Aug. 2017.

[8] H. Y. Kao, Z. X. Su, H. Sh. Shih, Y. Ch. Chi, Ch. T. Tsai, H. C. Kuo, Ch. H. Wu, J. J. Jou, T. T. Shih, and G. R. Lin, "CWDM DFBLD transmitter module for 10-km interdata center with single-channel 50-Gbit/s PAM-4 and 62-Gbit/s QAM-OFDM," IEEE Journal of Lightwave Technology, vol. 36, no. 3, pp. 703-711, Feb. 2018.

[9] J. Zhang, J. Yu, F. Li, N. Chi, Z. Dong, and X. Li, "11 × 5 × 9.3Gb/s WDM-CAP-PON based on optical single-side band multi-level multi-band carrier-less amplitude and phase modulation with direct detection," Optics Express, vol. 21, no. 16, pp. 188621-18848, Aug. 2013.

[10] Y. Sun, R. L. Jr., R. Shubochkin, A. H. McCurdy, K. Balemarthy, D. Braganza, J. Kamino, T. Gray, W. Fan, K. Wade, F. Chang, D. Gazula, G. Landry, J. Tatum, and S. Bhoja, "SWDM PAM4 transmission over next generation wide-band multimode optical fiber," IEEE Journal of Lightwave Technology, vol. 35, no. 4, pp. 690-697, Feb. 2015.

[11] C. Prodaniuc, N. Stojanovic, F. Karinou, Z. Qiang, and R. Llorente, "Performance comparison between 4D trellis coded modulation and PAM-4 for low-cost 400 Gbps WDM optical networks," IEEE Journal of Lightwave Technology, vol. 34, no. 22, pp. 5308-5316, Nov. 2016.

[12] F. Gao, S. Zhou, X. Li, S. Fu, L. Deng, M. Tang, D. Liu, and Q. Yang, "2 × 64 Gb/s PAM-4 transmission over 70 km SSMF using O-band 18G-class directly modulated lasers (DMLs)," Optics Express, vol. 25, no. 7, pp. 7230-7237, Apr. 2017.

[13] P. E. D. Cruz, T. M. F. Alves, and A. V. T. Cartaxo, "Virtual carrier-assisted DD-MB-OFDM schemes for UDWDM met-ro-access networks with improved tolerance to four-wave mixing," IEEE Journal of Lightwave Technology, vol. 35, no. 20, pp. 4468-4478, Oct. 2017.

[14] J. L. Wei, J. D. Ingham, D. G. Cunningham, R. V. Penty, and I. H. White, "Performance and power dissipation comparisons between 28 Gb/s NRZ, PAM, CAP and optical OFDM sys-tems for data communication applications," IEEE Journal of Lightwave Technology, vol. 30, no. 20, pp. 3273-3280, Oct. 2012.

[15] P. N. Ji, D. Qian, K. Kanonakis, C. Kachris, and I. Tom-kos, "Design and evaluation of a flexible-bandwidth OFDM-based intra-data center interconnect," IEEE Journal of Selected Topics In Quantum Electronics, vol. 19, no. 2, Article no. 3700310, Mar./Apr. 2013.

[16] X. Q. Liu, H. H. Chen, B. Y. Lyu, and W. X. Meng, " Symbol cyclic shift equalization PAM-OFDM a low complexity CP-free OFDM scheme." IEEE Transactions on Vehicular Technology, vol. 66, no. 7, pp. 5933-5946, Jul. 2017.

[17] J. Shi, J. Zhang, N. Chi and J. Yu, "Comparison of 100G PAM-8, CAP-64 and DFTS OFDM with a band-width-limited direct-detection receiver," Optics Express, vol. 25, no. 26, pp. 32254-32262, Dec. 2017.

[18] N. S. Andr´e, H. Louchet, V. Filsinger, E. Hansen, and A. Richter, "OFDM and PAM comparison using a high baudrate low resolution IM/DD interface for 400G Ethernet access," Optics Express, vol. 24, no. 11, pp. 11927-11931, May. 2016.

[19] J. Shi, J. Zhang, Y. Zhou, Y. Wang, N. Chi and Jianjun Yu, "Transmission performance comparison for 100-Gb/s PAM-4, CAP-16, and DFT-S OFDM with direct detection," IEEE Journal of Lightwave Technology, vol. 35, no. 23, pp. 5127-5133, Dec. 2017.

[20] D. J. F. Barros, S. K. Wilson and J. M. Kahn, "Comparison of orthogonal frequency-division multiplexing and pulse-amplitude modulation in indoor optical wireless links," IEEE Transactions on Communications, vol. 60, no. 1, pp. 153-163, Jan. 2012.

[21] R. Asifa, and M. Haithemc, "10 Gbit/s mode-multiplexed QPSK transmission using MDM-to-MFDM based single coherent receiver for intra- and inter data center networking," Optics Communications, vol., no., pp. 106-110, Jan. 2017.

[22] D. L. Butler, M. Ju. Li, Sh. Li, Y. Geng, R. R. Khrapko, R. A. Modavis, V. N. Nazarov and A. V. Koklyushkin, "Space division multiplexing in short reach optical interconnects," Journal of Lightwave Technology, vol. 35, no. 4, pp. 677-682, Feb. 2017.

[23] H. Yuan, M. Furdek, A. Muhammad, A. Saljoghei, L. Wosinska, and G. Zervas, "Space-division multiplexing in data center networks: on multi-core fiber solutions and cross-talk-suppressed resource allocation," IEEE Journal of Optical Communication and Networking, vol. 10, no. 4, pp. 272-288, Apr. 2018.

[24] T. Mizuno, H. Takara, A. Sano and Y. Miyamoto, "Dense space-division multiplexed transmission systems using multi-core and multimode fiber," IEEE Journal of Lightwave Technology, vol. 34, no. 2, pp. 582-592, Jan. 2016.

[25] A. Grieco, G. Porter, and Y. Fainman, "Integrated space-division multiplexer for application to data center net-works," IEEE Journal of Selected Topics in Quantum Electronics, vol. 22, no. 6, Article no. 8200106, Dec. 2016.

[26] Z. Zhu, Sh. Zhong, L. Chen, and K. Chen, "Fully programmable and scalable optical switching fabric for petabyte data center," Optics Express, vol. 23, no. 3, pp. 3563-3580, Feb. 2015.

[27] L. Xue, L. Yi, H. Ji, P. Li, and W. Hu, "Symmetric 100-Gb/s TWDM-PON in O-band based on 10G-class optical devices enabled by dispersion-supported equalization," IEEE Journal of Lightwave Technology, vol. 36, no. 2, pp. 580-586, Jan. 2018.

[28] F. Bao, T. Morioka, L. K. Oxenløwe, and H. Hu1, "300 Gb/s IM/DD based SDM-WDM-PON with laserless ONUs," Optics Express, vol. 26, no. 7, pp. 7949-7954, Apr. 2018.

[29] R. Lin, J. V. Kerrebrouck, X. Pang, M. Verplaetse, O. Ozolins, A. Udalcovs, L. Zhang, L. Gan, M. Tang, S. Fu, R. Schatz, U.

Westergren, S. Popov, D. Liu, W. Tong, T. D. Keulenaer, G. Torfs, J. Bauwelinck, X. Yin, and J. Chen, "Real-time 100 Gbps/λ/core NRZ and EDB IM/DD transmission over multi-core fiber for intra-datacenter communication networks," Optics Express, vol. 26, no. 8, pp. 10519-10526, Apr. 2018.

[30] T. N. Huynh, R. Watts, V. Vujicic, M. D. G. Pascual, C. Calo, K. Merghem, V. Panapakkam, F. Lelarge, A. Martinez, B. E. Benkelfat, A. Ramdane and L. P. Barry, "200-Gb/s bau-drate-pilot-aided QPSK/direct detection with single-section quantum-well mode-locked laser," IEEE Photonics Journal, vol. 8, no. 2, Article no. 7903107, Apr. 2016.

[31] H. Mardoyan, M. A. Mestre, J. M. Estar´an, F. Jorge, F. Blache, P. Angelini, A. Konczykowska, M. Riet, V. Nodji-adjim, J. Dupuy, and S. Bigo, "84-, 100-, and 107-GBd PAM-4 intensity modulation direct-detection transceiver for datacenter interconnects", IEEE Journal of Lightwave Technology, vol. 35, no. 6, pp. 1253-1259, Mar. 2017.

[32] H. Mardoyan, M. A. Mestre, R. Rios-M¨uller, A. Konczykowska, J. Renaudier, F. Jorge, B. Duval, J. Y. Dupuy, A. Ghazisaeidi, Ph. Jennev´e, M. Achouche, and S. Bigo, "Single carrier 168-Gb/s line-rate PAM direct detection transmission using high-speed selector power DAC for optical interconnects", IEEEE Journal of Lightwave Technology, vol. 34, no. 7, pp. 1593-1598, Apr. 2016.

[33] H. Y. Chen, N. Kaneda, J. Lee, J. Chen, and Y. K. Chen1, "Optical filter requirements in an EML-based single-sideband PAM4 intensity-modulation and direct-detection transmission system," Optics Express, vol. 25, no. 6, pp. 2852-2860, Mar. 2017.

[34] N. Suzuki, H. Miura, K. Matsuda, R. Matsumoto, and K. Mo-toshima, "100 Gb/s to 1 Tb/s based coherent passive optical network technology," IEEE Journal of Lightwave Technology, vol. 36, no. 8, pp. 1485-1491, Apr. 2018.

[35] J. Cai, H. G. Batshon, M. V. Mazurczyk, O. V. Sinkin, D. Wang, M. Paskov, W. W. Patterson, C. R. Davidson, P. C. Corbett, G. M. Wolter, T. E. Hammon, M. A. Bolshtyansky, D. G. Foursa and A. N. Pilipetskii, "70.46 Tb/s over 7,600 km and 71.65 Tb/s over 6,970 km transmission in C+L band using coded modulation with hybrid constellation shaping and non-linearity compensation," IEEE Journal of Lightwave Technology, vol. 36, no. 1, pp. 114-121, Jan. 2018.

[36] V. Houtsma and D. V. Veen, "Bi-directional 25G/50G TDM-PON with extended power budget using 25G APD and coherent detection," IEEE Journal of Lightwave Technology, vol. 36, no. 1, pp. 122-127, Jan. 2018.

[37] R. V. D. Linden, N. C. Tran, E. Tangdiongga, and T. Koo-nen, "Optimization of flexible non-uniform multilevel PAM for maximizing the aggregated capacity in PON deployments," IEEE Journal of Lightwave Technology, vol. 36, no. 12, pp. 2328-2336, June. 2018.

[38] X. Guo, D. G. Cunningham, R. V. Penty, and I. H. White, "Optical equalizers for bandwidth-limited transmitters and PAM-based fiber optic links," IEEE Journal of Lightwave Technology, vol. 36, no. 12, pp. 2484-2491, June. 2018.

[39] Z. Li, A. Tan, Y. Song, Y. Li, J. Chen, and M. Wang, " OOK-assisted adaptive equalization and timing recovery for PAM4 demodulation," IEEE Photonics Journal, vol. 10, no. 2, Article no. 7201607, Apr. 2018.

[40] I. N. Osahon, M. Safari, and W. O. Popoola, "10-Gb/s trans-mission over 10-m SI-POF with M-PAM and multilayer per-ceptron equalizer," IEEE Photonics Technology Letters, vol. 30, no. 10, pp. 911-914, May 2018.

[41] L. Tao, Y. Wang, Y. Gao, and N. Chi, "High order CAP system using DML for short reach optical communications," IEEE Photonics Technology Letters, vol. 26, no. 13, pp. 1348-1351, July 2014.

[42] Q. Chen, J. He, R. Deng, M. Chen, and L. Chen, "FFT-size efficient 4096-QAM OFDM for low-cost DML-based IMDD system," IEEE Photonics Journal, vol. 8, no. 5, Article no. 7804010, Aug. 2016.

[43] Q. Chen, J. He, R. Deng, M. Chen, and L. Chen, "FFT-size efficient 4096-QAM OFDM for low-cost DML-based IMDD system," IEEE Photonics Journal, vol. 8, no. 5, Article no. 7804010, Oct. 2016.

[44] X. Miao, M. Bi, Y. Fu, L. Li, and W. Hu, "Experimental study of NRZ, duobinary, and PAM-4 in O-band DML-based 100G-EPON," IEEE Photonics Technology Letters, vol. 29, no. 17, pp. 1490-1493, Sept. 2017.

[45] L. Tao, Y. Wang, J. Xiao, and N. Chi, "Enhanced performance of 400 Gb/s DML-based CAP systems using optical filtering technique for short reach communication," Optics Express, vol. 22, no. 24, pp. 29331-29339, Dec. 2014.

[46] T. C. Tzu, Y. Hsu, C. Y. Chuang, X. Wu, C. W. Chow, J. Chen, C. H. Yeh, and H. K. Tsang, "Equalization of PAM-4 signal generated by silicon microring modulator for 64-Gbit/s transmission," IEEE Journal of Lightwave Technology, vol. 35, no. 22, pp. 4943-4948, Nov. 2017.

[47] J. P. V. Engelen, L. Shen, G. Roelkens , Y. Jiao, M. K. Smit, and J. J. G. M. V. D. Tol, "A novel broadband electro-absorption modulator based on bandfilling in n-InGaAs: design and simulations," IEEE Journal of Selected Topics in Quantum Electronics, vol. 24, no. 1, Article no. 3300108, Jan/Feb. 2018.

[48] N. H. Zhu, Z. Shi, Z. K. Zhang, Y. M. Zhang, C. W. Zou, Z. P. Zhao, Y. Liu, W. Li, and M. Li, "Directly modulated semiconductor lasers." IEEE Journal of Selected Topics in Quan-tum Electronics, vol. 24, no. 1, Article no. 1500219, Jan/Feb. 2018.

[49] J. C. Cartledge and A. S. Karar, "100 Gb/s intensity modula-tion and direct detection," IEEE Journal of Lightwave Technology, vol. 32, no. 16, pp. 2809-2814, Aug. 2014.

[50] A. Abbasi, J. Verbist, L. A. Shiramin, M. Verplaetse, T. De Keulenaer, R. Vaernewyck, R. Pierco, A. Vyncke, X. Yin, G. Torfs, G. Morthier, J. Bauwelinck, and G. Roelkens, "100-Gb/s electro-absorptive duobinary modulation of an InP-on-Si DFB laser," IEEE Photonics Technology Letters, vol. 30, no. 12, pp. 1095-1098, Jun. 2018.

[51] S. K. Kang, J. Y. Huh, J. H. Lee, and J. K. Lee, "Low-cost and miniaturized 100-Gb/s (2 × 50 Gb/s) PAM-4 TO-packaged ROSA for data center networks," Optics Express, vol. 26, no. 5, pp. 6172-6181, Mar. 2018.

[52] J. Chen, Z. S. He, T. Lengyel, K. Szczerba, P. Westbergh, J. S. Gustavsson, H. Zirath, and A. Larsson, "An energy efficient 56 Gbps PAM-4 VCSEL transmitter enabled by a 100 Gbps driver in 0.25 μm InP DHBT technology," IEEE Photonics

Technology Letters, vol. 34, no. 21, pp. 4954-4964, Nov. 2016.

[53] B. D. Feris, Ph. Gravey, P. Morel, M. L. Moulinard, M. Morvan, and A. Sharaiha, "Dimensioning of 112G optical-packet-switching-based interconnects for energy-efficient data centers," IEEE Journal of Optical Communication and Networking, vol. 9, no. 4, pp. B124-B136, Apr. 2017.

[54] J. Shi, J. Zhang, Y. Zhou, Y. Wang, N. Chi, and J. Yu, "Transmission performance comparison for 100-Gb/s PAM-4, CAP-16, and DFT-S OFDM with direct detection," IEEE Journal of Lightwave Technology, vol. 35, no. 23, pp. 5127-5133, Dec. 2017.

[55] S. Kanazawa, Y. Nakanishi, S. Tsunashima, H. Yamazaki, Y. Ueda, W. Kobayashi, Y. Muramoto, H. Ishii, and H. Sanjoh, "Equalizer-free transmission of 100-Gb/s 4-PAM signal generated by flip-chip interconnection EADFB laser module," IEEE Journal of Lightwave Technology, vol. 35, no. 4, pp. 775-780, Feb. 2017.

[56] L. Xue, L. Yi, H. Ji, P. Li, and W. Hu, "Symmetric 100-Gb/s TWDM-PON in O-band based on 10G-class optical devices enabled by dispersion-supported equalization," IEEE Journal of Lightwave Technology, vol. 36, no. 2, pp. 580-586, Jan. 2018.

[57] K. Fang, J. Yu, H. Wang, and X. Li, "56 Gbps signal generation from one 10-G class laser diode for 400G intra-data center interconnection," Optical Fiber Technology, vol. 36, pp. 210-214, Apr. 2017.

[58] R. R. M¨uller, J. Renaudier, P. Brindel, A. Ghazisaeidi, I. Fernandez, P. Tran, C. Simonneau, L. Schmalen, and G. Charlet, "Spectrally-efficient 400-Gb/s single carrier transport over 7 200 km," IEEE Journal of Lightwave Technology, vol. 33, no. 7, pp. 1402-1407, Apr. 2015.

[59] F. Karinou, N. Stojanovic, C. Prodaniuc, M. Agustin, J. Kropp, and N. N. Ledentsov, "Solutions for 100/400-Gb/s ethernet systems based on multimode photonic technologies," IEEE Journal of Lightwave Technology, vol. 35, no. 15, pp. 3214-3222, Aug. 2017.

[60] G. Khanna, T. Rahman, E. D. Man, E. Riccardi, A. Pagano, A. C. Piat, S. Calabrò, B. Spinnler, D. Rafique, U. Feiste, H. D. Waardt, B. S. Krombholz, N. Hanik, T. Drenski, M. Bohn, and A. Napoli, "Single-carrier 400G 64QAM and 128QAM DWDM field trial transmission over metro legacy links," IEEE Photonics Technology Letters, vol. 29, no. 2, pp. 189-192, Jan. 2017.

[61] J. M. F`abrega, M. S. Moreolo, A. Mayoral, R. Vilalta, R. Casellas, R. Mart´ınez, R. Mu¯noz, Y. Yoshida, K. Kitayama, Y. Kai, M. Nishihara, R. Okabe, T. Tanaka, T. Takahara, J. C. Rasmussen, N. Yoshikane, X. Cao, T. Tsuritani, I. Morita, K. Habel, R. Freund, V. L´opez, A. Aguado, S. Yan, D. Sime-onidou, T. Szyrkowiec, A. Autenrieth, M. Shiraiwa, Y. Awaji, and N. Wada, "Demonstration of adaptive SDN orchestration: a real-time congestion-aware services provisioning over OFDM-Based 400G OPS and Flexi-WDM OCS," IEEE Journal of Lightwave Technology, vol. 35, no. 3, pp. 506-512, Feb. 2017.

[62] Y. Nakanishi, T. Ohno, T. Yoshimatsu, and H. Sanjoh, "High-sensitivity 4-channel receiver module with avalanche photodiode for 400-Gbit/s Ethernet," NTT Technical, vol. 14, no. 9, pp. 1-6, Sept. 2016.

[63] P. Groumas, V. Katopodis, J. H. Choi, H. G. Bach, J. Y. Dupuy, A. Konczykowska, Z. Zhang, P. Harati, E. Miller, A. Beretta, L. Gounaridis, F. Jorge, V. Nodjiadjim, A. Dede, A. Vannucci, G. Cangini, R. Dinu, N. Keil, N. Grote, H. Avram-opoulos, and C. Kouloumentas, "Multi-100 GbE and 400 GbE interfaces for intra-data center networks based on arrayed transceivers with serial 100 Gb/s operation," IEEE Journal of Lightwave Technology, vol. 33, no. 4, pp. 943-954, Feb. 2015.

[64] N. Eiselt, J. Wei, H. Griesser, A. Dochhan, M. H. Eiselt, J. P. Elbers, J. J. V. Olmos, and I. T. Monroy, "Evaluation of re-al-time 8 × 56.25 Gb/s (sdG) PAM-4 for inter-data center application over 80 km of SSMF at 1550 nm," IEEE Journal of Lightwave Technology, vol. 35, no. 4, pp. 955-962, Feb. 2017.

[65] N. S. Andr´e, H. Louchet, V. Filsinger, E. Hansen, and A. Richter1, "OFDM and PAM comparison using a high bau-drate low resolution IM/DD interface for 400G Ethernet access," Optics Express, vol. 24, no. 11, pp. 11926-11931, May. 2016.

[66] C. Prodaniuc, N. Stojanovic, F. Karinou, Z. Qiang, and R. Llorente, "Performance comparison between 4D trellis coded modulation and PAM-4 for low-cost 400 Gbps WDM optical networks," IEEE Journal of Lightwave Technology, vol. 34, no. 22, pp. 5308-5316, Nov. 2016.

[67] R. Lin, J. V. Kerrebrouck, X. Pang, M. Verplaetse, O. Ozolins, A. Udalcovs, L. Zhang, L. Gan, M. Tang, S. Fu, R. Schatz, U. Westergren, S. Popov, D. Liu, W. Tong, T. D. Keulenaer, G. Torfs, J. Bauwelinck, X. Yin, and J. Chen, "Real-time 100 Gbps/λ/core NRZ and EDB IM/DD transmission over multi-core fiber for intra-datacenter communication networks," Op-tics Express, vol. 26, no. 8, pp. 10519-10526, Apr. 2018.

[68] X. Pang, O. Ozolins, S. Gaiarin, A. Kakkar, J. R. Navarro, M. I. Olmedo, R. Schatz, A. Udalcovs, U. Westergren, D. Zibar, S. Popov, and G. Jacobsen, "Experimental study of 1.55-μm EML-based optical IM/DD PAM-4/8 short reach systems," IEEE Photonics Technology Letters, vol. 29, no. 6, pp. 523-526, Mar. 2017.

[69] F. Karinou, N. Stojanovic, A. Daly, Ch. Neumeyr, and M. Ortsiefer, "1.55-μm long-wavelength VCSEL-based optical interconnects for short-reach networks," IEEE Journal of Lightwave Technology, vol. 34, no. 12, pp. 2897-2904, Jun. 2016.

[70] K. Zhong, X. Zhou, T. Gui, L. Tao, Y. Gao, W. Chen, J. Man, L. Zeng, A. P. T. Lau, and Ch. Lu, "Experimental study of PAM-4, CAP-16, and DMT for 100 Gb/s short reach optical transmission systems," Optics Express, vol. 23, no. 2, pp. 1176-1189, Jan. 2015.

[71] N. Eiselt, J. Wei, H. Griesser, A. Dochhan, M. H. Eiselt, J. P. Elbers, J. J. V. Olmos, and I. T. Monroy, "Evaluation of re-al-time 8x56.25 Gb/s (400G) PAM-4 for inter-data center ap-plication over 80 km of SSMF at 1550 nm," IEEE Journal of Lightwave Technology, vol. 35, no. 4, pp. 955-962, Feb. 2017.

[72] W. Miao, H. d. Waardt, R. v. d. Linden, and N. Calabretta, "Assessment of scalable and fast 1310-nm optical switch for high-capacity data center networks," IEEE Photonics Technology Letters, vol. 29, no. 1, pp. 98-101, Jan. 2017.

[73] M. Mosman, M. Chagnon, M. Poulin, S. Lessard, and D. V. Plant, "224-Gb/s 10-km transmission of PDM PAM-4 at 1.3 μm using a single intensity-modulated laser and a direct-detection MIMO DSP-based receiver," IEEE Journal of Lightwave Technology, vol. 33, no. 7, pp. 1417-1424, Apr. 2015.

[74] K. Zhong, X. Zhou, Y. Gao, W. Chen, J. Man, L. Zeng, A. P. T. Lau, and Ch. Lu, "140-Gb/s 20-km transmission of PAM-4 signal at 1.3 μm for short reach communications," IEEE Pho-tonics Technology Letters, vol. 27, no. 16, pp. 1757-1760, Aug. 2015.

[75] K. Szczerba, P. Westbergh, J. Karout, J. S. Gustavsson, Å. Haglund, M. Karlsson, P. A. Andrekson, E. Agrell, and A. Larsson, "4-PAM for high-speed short-range optical communications," Journal of Optical Communication and Networking, vol. 4, no. 11, pp. 885-894, Nov. 2012.